

## The Most Metal-poor Stars in Omega Centauri (NGC 5139)<sup>\*</sup>

CHRISTIAN I. JOHNSON,<sup>1</sup> ANDREA K. DUPREE,<sup>2</sup> MARIO MATEO,<sup>3</sup> JOHN I. BAILEY, III,<sup>4</sup> EDWARD W. OLSZEWSKI,<sup>5</sup> AND MATTHEW G. WALKER<sup>6</sup>

<sup>1</sup>Space Telescope Science Institute, 3700 San Martin Drive, Baltimore, MD 21218, USA

<sup>2</sup>Center for Astrophysics | Harvard & Smithsonian, 60 Garden Street, MS-15, Cambridge, MA 02138, USA

<sup>3</sup>Department of Astronomy, University of Michigan, Ann Arbor, MI 48109, USA

<sup>4</sup>Department of Physics, UCSB, Santa Barbara, CA 93016, USA

<sup>5</sup>Steward Observatory, The University of Arizona, 933 N. Cherry Avenue, Tucson, AZ 85721, USA

<sup>6</sup>McWilliams Center for Cosmology, Department of Physics, Carnegie Mellon University, 5000 Forbes Avenue, Pittsburgh, PA 15213, USA

(Received XXX; Revised XXX; Accepted XXX)

Submitted to AJ

### ABSTRACT

The most massive and complex globular clusters in the Galaxy are thought to have originated as the nuclear cores of now tidally disrupted dwarf galaxies, but the connection between globular clusters and dwarf galaxies is tenuous with the M54/Sagittarius system representing the only unambiguous link. The globular cluster Omega Centauri ( $\omega$  Cen) is more massive and chemically diverse than M 54, and is thought to have been the nuclear star cluster of either the Sequoia or Gaia-Enceladus galaxy. Local Group dwarf galaxies with masses equivalent to these systems often host significant populations of very metal-poor stars ( $[\text{Fe}/\text{H}] < -2.5$ ), and one might expect to find such objects in  $\omega$  Cen. Using high resolution spectra from Magellan-M2FS, we detected 11 stars in a targeted sample of 395 that have  $[\text{Fe}/\text{H}]$  ranging from  $-2.30$  to  $-2.52$ . These are the most metal-poor stars discovered in the cluster, and are  $5\times$  more metal-poor than  $\omega$  Cen's dominant population. However, these stars are not so metal-poor as to be unambiguously linked to a dwarf galaxy origin. The cluster's metal-poor tail appears to contain two populations near  $[\text{Fe}/\text{H}] \sim -2.1$  and  $-2.4$ , which are very centrally concentrated but do not exhibit any peculiar kinematic signatures. Several possible origins for these stars are discussed.

**Keywords:** globular clusters: general, globular clusters: individual: Omega Centauri, stars: abundances, stars: Population II, Astrophysics - Solar and Stellar Astrophysics

### 1. INTRODUCTION

Omega Centauri ( $\omega$  Cen) possesses an elegant complexity that is unmatched by any other Galactic globular cluster. While most globular clusters exhibit metallicity dispersions of  $\sim 0.05$  dex or less (e.g., Carretta et al. 2009; Bailin 2019), stars in  $\omega$  Cen span at least a factor of 100 in  $[\text{Fe}/\text{H}]^1$  and are distributed into at least 5 distinct popula-

tions with unique metallicities (e.g., Suntzeff & Kraft 1996; Norris & Da Costa 1995; Norris et al. 1996; Villanova et al. 2007; Johnson & Pilachowski 2010; Marino et al. 2011; Pancino et al. 2011b). Each distinct metallicity group can be further partitioned into at least 2-3 sub-populations with variable light element chemistry, and  $\omega$  Cen may host as many as 15 unique stellar populations (Bellini et al. 2017).

The origin and enrichment history of  $\omega$  Cen is currently an open question, but several lines of evidence suggest that the cluster may be the remnant core of a now disrupted dwarf galaxy. For example,  $\omega$  Cen is the brightest and most massive globular cluster in the Milky Way, but has a strong retrograde orbit (Dinescu et al. 1999) that may be associated with

Corresponding author: Christian I. Johnson  
 chjohnson@stsci.edu

\* This paper includes data gathered with the 6.5 meter Magellan Telescopes located at Las Campanas Observatory, Chile.

<sup>1</sup>  $[\text{A}/\text{B}] \equiv \log(\text{N}_\text{A}/\text{N}_\text{B})_\text{star} - \log(\text{N}_\text{A}/\text{N}_\text{B})_\odot$  for elements A and B.

the capture and disruption of the “Sequoia” galaxy discussed in Myeong et al. (2019). Alternatively,  $\omega$  Cen could have once been the nuclear star cluster of the more massive Gaia-Enceladus galaxy (Massari et al. 2019). Bekki & Freeman (2003) used dynamical models to show that a compact nuclear core like  $\omega$  Cen could survive such a disruption event, and in fact the long tidal stream recently found by Ibata et al. (2019), which stretches several degrees along the cluster’s orbit, seems to support an accretion origin (see also Simpson et al. 2019). We also note that  $\omega$  Cen shares many physical and chemical characteristics with M 54 (e.g., Carretta et al. 2010a), which is the most massive cluster in the Sagittarius dwarf galaxy that is currently being tidally destroyed by the Milky Way.

In terms of size and luminosity,  $\omega$  Cen and M 54 lie at the intersection between globular clusters, nuclear star clusters, and Ultra Compact Dwarfs (e.g., Mackey & van den Bergh 2005; Georgiev et al. 2009; Tolstoy et al. 2009), and may be prototypes for “iron-complex” clusters<sup>2</sup> that host multiple generations of stars with different light and heavy element abundances (e.g., Yong et al. 2014; Johnson et al. 2015a; Marino et al. 2015; Da Costa 2016; Milone et al. 2017). Although a definitive connection between iron-complex clusters and dwarf galaxy nuclei has not yet been established (e.g., see Da Costa 2016), one possible investigation path is to search for cluster members that may have originally been part of the progenitor galaxy’s field star population. Such stars could be identified as having chemistry that is inconsistent with known globular cluster patterns.

For  $\omega$  Cen, the two most likely populations to have originated as dwarf galaxy field stars are those at the highest ( $[Fe/H] \gtrsim -1$ ) and lowest ( $[Fe/H] \lesssim -2$ ) metallicities. On the high metallicity end, stars exhibit relatively small light element abundance variations and critically show an O-Na correlation rather than the expected anti-correlation (Johnson & Pilachowski 2010; Marino et al. 2011; Pancino et al. 2011a). However, several authors have noted that this particular pattern may be attributed to self-enrichment driven by an unusually long star formation history (Johnson & Pilachowski 2010; D’Antona et al. 2011; Marino et al. 2011). The iron-complex clusters M 2 (Yong et al. 2014) and NGC 6273 (Johnson et al. 2015a, 2017) also contain minority populations of metal-rich stars with small star-to-star abundance variations, but in these cases no clear O-Na

correlations are present. For all three clusters the origins of their metal-rich populations remain ambiguous, and it is not yet possible to differentiate whether these stars were captured from a progenitor galaxy or simply trace prolonged chemical enrichment.

The most metal-poor  $\omega$  Cen stars have a greater potential to unambiguously link the cluster with a dwarf galaxy formation environment. For example, Milky Way and extragalactic globular cluster systems exhibit a clear metallicity floor of  $[Fe/H] \sim -2.3$  to  $-2.5$  (e.g., Beasley et al. 2019), which suggests that any  $\omega$  Cen stars more metal-poor than this limit likely did not originate in the cluster. The metallicity distribution function of the Sequoia galaxy, proposed by Myeong et al. (2019) as the progenitor system for  $\omega$  Cen, is not currently well-constrained, but several estimates indicate that it likely had a mass in excess of  $10^7 M_{\odot}$  (e.g., Bekki & Tsujimoto 2019; Myeong et al. 2019). The dwarf galaxy mass-metallicity relation from Kirby et al. (2013) suggests that such a system should have a mean  $[Fe/H] \sim -1.5$ , but if  $\omega$  Cen formed in a  $10^{10} M_{\odot}$  system, such as Gaia-Enceladus (Helmi et al. 2018), then the host galaxy’s mean metallicity may have been closer to  $[Fe/H] \sim -0.5$ . In either case, the metallicity distribution functions of most existing dwarf galaxies exhibit long metal-poor tails that reach at least 1-2 dex lower than their mean  $[Fe/H]$  values (e.g., Starkenburg et al. 2010; Kirby et al. 2011; Leaman et al. 2013), which suggests that any dwarf galaxy massive enough to host  $\omega$  Cen likely had  $\sim 1$ -10% of its stars with  $[Fe/H] \lesssim -2.5$ .

Previous analyses of  $\omega$  Cen’s red giant branch (RGB) and subgiant branch (SGB) populations have so far failed to find any stars with  $[Fe/H] \lesssim -2.25$ , which is still within the metallicity realm of Galactic globular clusters. Recent RR Lyrae investigations by Bono et al. (2019) and Magurno et al. (2019) found a small number of stars with  $[Fe/H] \lesssim -2.5$ ; however, the mean cluster metallicities of these studies are  $\sim 0.2$ -0.3 dex lower than spectroscopic analyses of RGB stars (e.g., Johnson & Pilachowski 2010), which suggests their true metallicity floor may be closer to  $[Fe/H] \sim -2.3$ .

Broad-band color-magnitude diagram analyses alone are unlikely to find very low metallicity stars in  $\omega$  Cen because the RGB evolutionary sequences of old populations become difficult to distinguish in color below  $[Fe/H] \sim -2$  (e.g., see Figure 7 of Simpson 2018). Furthermore, the isochrones of very metal-poor RGB stars in  $\omega$  Cen may overlap in color and magnitude space with asymptotic giant branch (AGB) sequences as well. Many of the bluer  $\omega$  Cen stars, especially in regions where RGB and AGB stars of different metallicity can mix, do not yet have spectroscopic  $[Fe/H]$  determina-

<sup>2</sup> Note that iron-complex clusters are generally the same as the “anomalous” and “Type II” clusters identified by Marino et al. (2015) and Milone et al. (2017), respectively.

tions, and as a result the most metal-poor stars in the cluster may have been missed by previous surveys. Therefore, we derive spectroscopic [Fe/H] measurements for 395 of the bluest RGB stars in  $\omega$  Cen to search for the cluster's most metal-poor constituents that may link the system to formation in a dwarf galaxy environment.

## 2. OBSERVATIONS AND DATA REDUCTION

All spectroscopic data for this project were obtained using the Michigan-Magellan Fiber System (M2FS; Mateo et al. 2012) and MSpec spectrograph mounted on the Magellan-Clay 6.5m telescope at Las Campanas Observatory. The spectra were acquired in three runs via the M2FS queue that spanned 2015 February 19, 21, 22, 23, and 25 for the first set, 2015 March 01, 02, and 04 for the second set, and 2015 July 18 and 20 for the third set. Ten different fiber configurations were used for seven unique pointings, which are illustrated in the right panel of Figure 1. Three of the fields that overlapped with the cluster core included two separate fiber configurations in order to maximize the number of observed stars. The remaining 4 fields each only included a single fiber configuration.

Target stars were selected using the photometry and coordinates from van Leeuwen et al. (2000). Only objects identified by van Leeuwen et al. (2000) as having membership probabilities  $> 70\%$  were targeted, and we prioritized stars on the blue half of the RGB with V magnitudes between about 13.5 and 14.5 (see Figure 1). Although most stars in our sample are first ascent RGB stars, we also included some AGB and red horizontal branch (HB) stars since the isochrones for very metal-poor RGB stars are difficult to distinguish from these later evolutionary stages in more metal-rich populations. Including all configurations, fibers were placed on 458 unique targets spanning a variety of cluster radii (see Figure 1; Table 1); however, we were only able to measure [Fe/H] values for 395 targets. The remaining 63 targets had poor S/N spectra, were heavily blended spectroscopic binaries, or were cases in which we could not converge to a stable model atmosphere solution.

All observations utilized the “Mg\_Wide” filters that permit continuous wavelength coverage from approximately 5125–5410 Å. This particular setup was chosen because we are searching for stars with  $[Fe/H] \lesssim -2.3$  and the Fe lines in this region remain detectable in the spectra of  $T_{eff} \sim 5000$  K RGB stars down to at least  $[Fe/H] = -4$  (e.g., see Figure 1 of Frebel et al. 2015). The “red” and “blue” spectrographs employed identical configurations with  $1 \times 2$  (dispersion  $\times$  spatial) CCD binning, 95μm slits, a four amplifier slow readout, and provided a resolving power of  $R \equiv \lambda/\Delta\lambda \approx 32,000$ . Since

the Mg\_Wide filter spans four consecutive orders, we were only able to observe a maximum of 24 targets per spectrograph at a time. Each fiber configuration was observed for one hour with a set of  $3 \times 1200$  second exposures.

The data reduction procedure generally followed the methods outlined in Johnson et al. (2015b). Briefly, the IRAF<sup>3</sup> *CCDPROC* routine was used to apply the bias corrections, trim the overscan regions, and subtract dark current for each amplifier image. The *IMTRANSPPOSE* and *IMJOIN* routines were then used to align and combine the four amplifier images of every exposure to create sets of monolithic 2K×4K images. The *DOTHYDRA* task was utilized to handle aperture identification, aperture tracing, flat-fielding, wavelength calibration via ThAr comparison spectra, scattered light and cosmic ray removal, throughput corrections, and spectrum extraction. Median sky spectra were generated for each order on each night from the designated sky fiber data, and were subtracted from the appropriate science spectra. The sky subtracted data were then corrected for heliocentric velocity variations, continuum normalized, and median combined. Sample combined spectra for several stars with different [Fe/H] but similar temperature and surface gravity values are provided in Figure 2. Signal-to-noise (S/N) ratios for the combined spectra ranged from  $\sim 20$ –50 per reduced pixel.

## 3. DATA ANALYSIS

### 3.1. Model Atmospheres

For consistency with the Johnson & Pilachowski (2010) temperature/gravity scale, model atmosphere parameters were determined for each star using dereddened B, V, and K<sub>S</sub>-band photometry from van Leeuwen et al. (2000) and the Two Micron All Sky Survey (2MASS; Skrutskie et al. 2006). Although several authors note the existence of minor ( $\Delta \sim 0.02$  mag.) differential reddening near the cluster core (e.g., Calamida et al. 2005; van Loon et al. 2007; McDonald et al. 2009), we assumed a constant  $E(B-V) = 0.11$  (Calamida et al. 2005) across the cluster and also utilized the relation  $E(V-K_S)/E(B-V) = 2.70$  from McCall (2004). For target stars with clear 2MASS matches, effective temperatures ( $T_{eff}$ ) were determined using the  $V-K_{TCS}$  color-temperature relation from

<sup>3</sup> IRAF is distributed by the National Optical Astronomy Observatory, which is operated by the Association of Universities for Research in Astronomy, Inc., under cooperative agreement with the National Science Foundation.

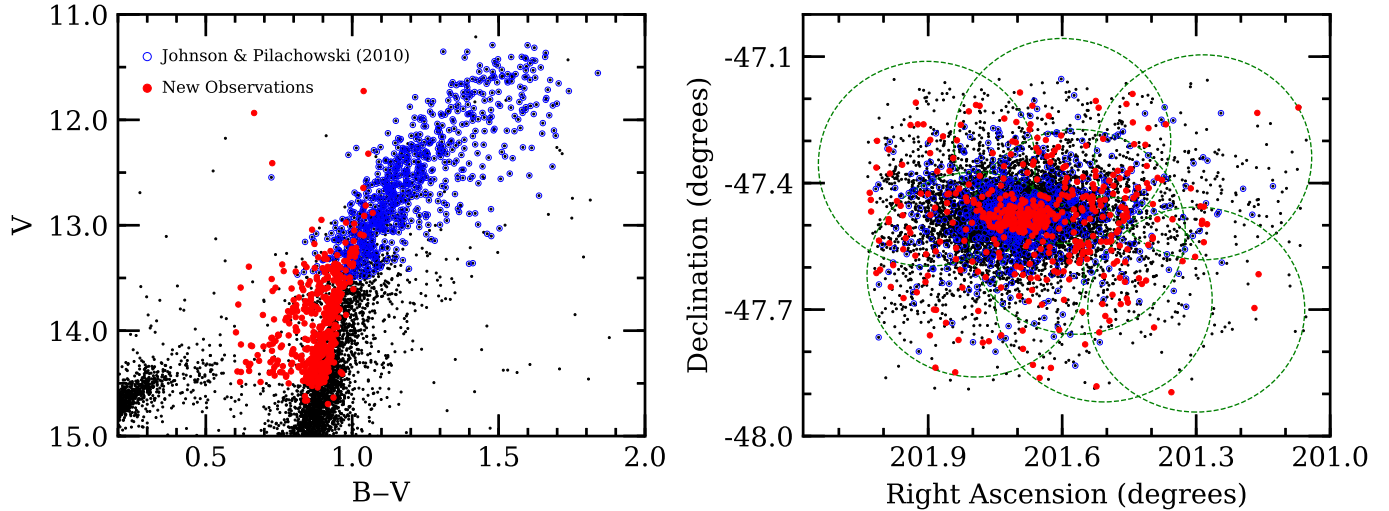


**Figure 1.** The left panel shows a V versus B–V color-magnitude diagram for all stars with membership probabilities  $> 70\%$  in the van Leeuwen et al. (2000) catalog. Stars observed in Johnson & Pilachowski (2010) and the present study are indicated with open blue circles and filled red circles, respectively. The right panel uses the same symbols to illustrate the sky coordinates of the targets observed in both spectroscopic studies. The M2FS configuration fields are identified with green dashed circles.

Alonso et al. (1999)<sup>4</sup>. In the few cases where clear 2MASS matches could not be obtained we used the B–V color-temperature relation from Alonso et al. (1999) to derive  $T_{\text{eff}}$  values. The estimated  $T_{\text{eff}}$  uncertainty is approximately 30 K for temperatures derived from V– $K_{\text{TCS}}$  and 130 K for B–V, based on the scatter of the empirical color-temperature relations in Alonso et al. (1999, see their Table 2).

Similar to  $T_{\text{eff}}$ , surface gravity ( $\log g$ ) values were determined for each star using photometric temperatures and absolute bolometric magnitudes ( $M_{\text{bol}}$ ). The bolometric magnitude values were calculated using the corrections provided by Alonso et al. (1999) and a distance modulus of  $(m-M)_V = 13.7$  (van de Ven et al. 2006). Final surface gravity values were determined using the relation,

$$\log(g_*) = 0.40(M_{\text{bol}} - M_{\text{bol},\odot}) + \log(g_{\odot}) + (1)$$

$$4[\log(\frac{T}{T_{\odot}})] + \log(\frac{M}{M_{\odot}}),$$

where we assumed a mass of  $0.8 M_{\odot}$  for all stars. Although a mass of  $0.8 M_{\odot}$  is a reasonable assumption for most cluster RGB stars, Figure 1 shows that some of our targets may be lower mass AGB or red HB stars. McDonald et al. (2011) showed that  $\omega$  Cen RGB stars lose  $\sim 25\%$  of their mass between the RGB and AGB sequences so a significant fraction of our targets may have masses closer to  $0.6 M_{\odot}$ . Fortunately, the photometric

surface gravity estimate shown above is only sensitive to the log of the mass difference, and we have restricted the present analysis to only include Fe I lines, which are not strongly pressure sensitive in the stars targeted here. Assuming the difference between RGB and AGB masses does not exceed  $\sim 0.2 M_{\odot}$ , we adopt a  $\log(g)$  uncertainty of 0.15 (cgs).

For most stars in our analysis, the available Fe I lines are too strong to tightly constrain the microturbulence ( $\xi_{\text{mic}}$ ). Therefore, we determined an empirical relation between  $T_{\text{eff}}$  and  $\xi_{\text{mic}}$  as,

$$\xi_{\text{mic}} = -6.46 \times 10^{-4} T_{\text{eff}} + 4.66, \quad (2)$$

using data from Johnson & Pilachowski (2010) that spanned the same  $T_{\text{eff}}$  range as the stars presented here. The adopted microturbulence calibration has a dispersion of  $0.17 \text{ km s}^{-1}$ .

Since the photometric color-temperature relation is dependent on metallicity and the surface gravity and microturbulence estimates require accurate temperature measurements, generating a global model atmosphere solution for each star is an iterative process. Therefore, we initially determined  $T_{\text{eff}}$ ,  $\log(g)$ , and  $\xi_{\text{mic}}$  for each star assuming  $[\text{Fe}/\text{H}] = -1.7$ , and iteratively solved for all four parameters as the metallicity determination improved (see also §3.3). We interpolated within the ATLAS9 grid of model atmospheres from Castelli & Kurucz (2003), and in general a stable solution was reached after  $\sim 3$  iterations. The adopted model atmosphere parameters,  $[\text{Fe}/\text{H}]$  values, photometry, star identifiers, and coordinates are provided in Table 1.

<sup>4</sup> Note that the 2MASS  $K_{\text{s}}$ -band photometry were transformed onto the  $K_{\text{TCS}}$  system using the transformations listed in Johnson et al. (2005).

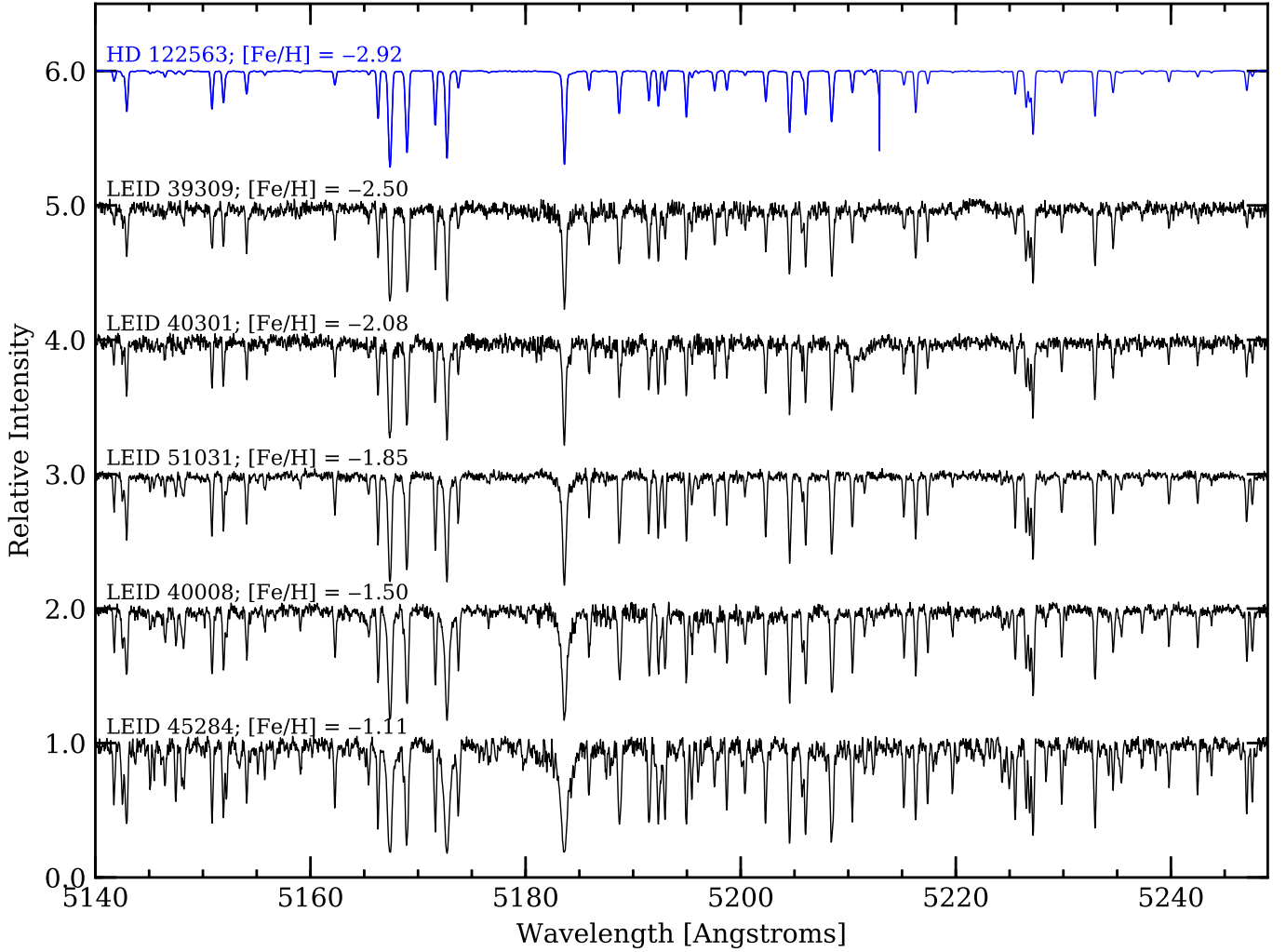


**Figure 2.** Sample M2FS spectra (black lines) are shown for  $\omega$  Cen stars that span  $[Fe/H] = -2.50$  to  $-1.11$  in increments of approximately 0.35 dex. A smoothed and resampled MIKE spectrum of the metal-poor giant HD 122563 is shown in blue for comparison. Note that all of the stars illustrated here have similar temperature and surface gravity values. A simple line strength comparison shows that LEID 40301 and LEID 39309 are clearly more metal-poor than LEID 51031, which represents the dominant  $\omega$  Cen population, but do not reach the very low level of  $[Fe/H] = -2.92$  found by Afsar et al. (2016) for HD 122563.

### 3.2. Membership and Radial Velocities

Although cluster membership probabilities were provided by van Leeuwen et al. (2000) based on proper motion measurements, we verified membership using radial velocity measurements as well. Radial velocities were determined using the first exposure of each configuration and comparing it with a synthetic reference spectrum at rest velocity that matched the resolution and sampling of the data. The observed radial velocity values were determined using the *XCSAO* routine from Kurtz & Mink (1998), and heliocentric corrections were calculated using IRAF's *rvcor* routine. The final heliocentric radial velocities and *XCSAO* error measurements for each star are provided in Table 1.

We found a mean heliocentric radial velocity of  $+232.5 \text{ km s}^{-1}$  for  $\omega$  Cen with a dispersion of  $12.8 \text{ km s}^{-1}$ . These values are in good agreement with previous work (e.g., Reijns et al. 2006; Sollima et al. 2009). A direct comparison of stars in common between this work and Reijns et al. (2006) gives a mean velocity difference, in the sense of the present work minus the literature, of  $+1.0 \text{ km s}^{-1}$  with a dispersion of  $1.7 \text{ km s}^{-1}$  (55 stars). A similar comparison with Sollima et al. (2009) gives a mean difference of  $+2.2 \text{ km s}^{-1}$  and a dispersion of  $2.9 \text{ km s}^{-1}$  (215 stars). The data presented in Table 1 indicate a radial velocity range spanning  $+186.7$  to  $+271.1 \text{ km s}^{-1}$ ; however, given the cluster's high radial velocity relative to the background and its large velocity

dispersion, we designate all stars in our sample as cluster members<sup>5</sup>.

### 3.3. $[Fe/H]$ Determinations

Given the modest S/N ratios of the spectra and the small number of available Fe II lines, all iron abundance determinations were made using synthetic spectrum fits to Fe I features. We first selected a subset of 14 Fe I lines between 5140 and 5390 Å that were visible in a majority of our spectra but had typical equivalent widths lower than about 150 mÅ. The spectrum synthesis line lists were augmented to include significant lines within 5 Å of each Fe I feature listed in Table 2. Due to a paucity of high accuracy experimental log gf values for the features given in Table 2, empirical log gf values were determined for all lines by first adopting atomic data from the Vienna Atomic Line Database (Ryabchikova et al. 2015) compilation and then adjusting the log gf values until a satisfactory fit to an M2FS daylight solar spectrum was achieved. We adopted the Anders & Grevesse (1989) solar abundances for all elements<sup>6</sup>. Although MgH lines may be present at wavelengths bluer than  $\sim 5200$  Å, the roughly 4800 K temperatures and low metallicities of our stars inhibited significant molecular contamination. Furthermore, we only selected Fe I lines that were at least  $\sim 0.5$  Å away from significant molecular blends. As a result, the adopted line list only included atomic features. The adopted atomic parameters for all Fe I lines of interest are provided in Table 2.

As mentioned previously, an initial estimate of  $T_{\text{eff}}$ ,  $\log(g)$ , and  $\xi_{\text{mic}}$  was made for each star assuming  $[Fe/H] = -1.7$ . For the first iteration, the  $T_{\text{eff}}$ ,  $\log(g)$ , and  $\xi_{\text{mic}}$  values were held fixed while model atmospheres and synthetic spectra were generated for  $[Fe/H]$  values ranging from  $-2.75$  to  $-0.5$ , in 0.01 dex steps, using the LTE line analysis code MOOG (Sneden 1973). The fits for each line were visually inspected to identify and remove lines affected by spectrum flaws, to set appropriate smoothing/broadening parameters, and to remove extreme outliers ( $\gtrsim 0.3$  dex from the mean). The  $[Fe/H]$  abundance that minimized the fitting residuals between the synthetic and observed spectra was selected as the new metallicity parameter, which enabled an update to the  $T_{\text{eff}}$ ,  $\log(g)$ , and  $\xi_{\text{mic}}$  values. This process was repeated until the difference in mean  $[Fe/H]$  between consecutive runs decreased to  $< 0.03$  dex, and then a fi-

nal iteration was performed. The adopted  $[Fe/H]$  abundances for each star are provided in Table 1 and also summarized as a histogram in Figure 3.

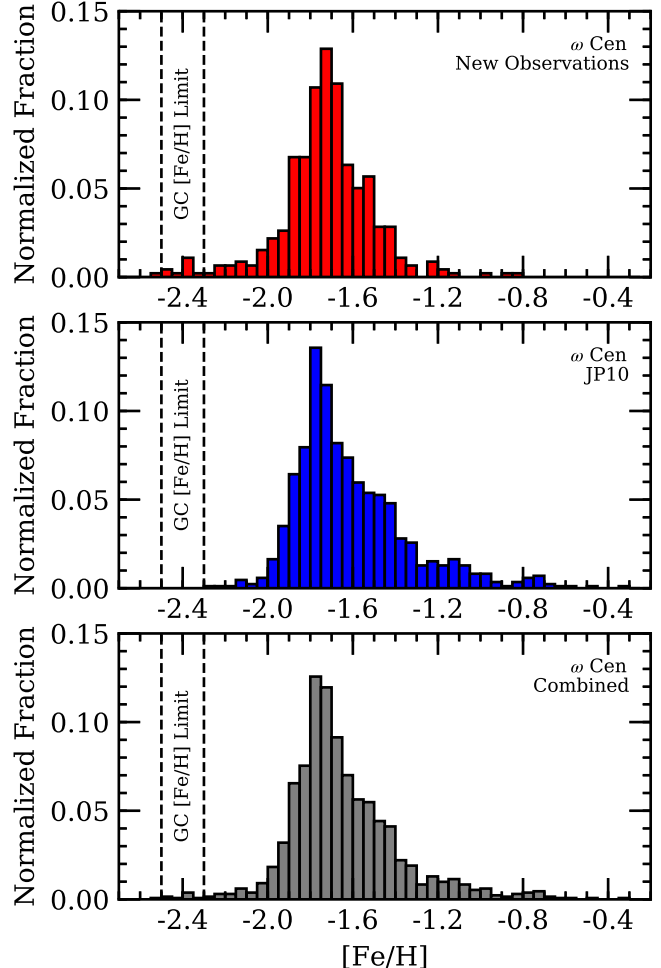


**Figure 3.** The top, middle, and bottom panels illustrate binned metallicity distribution functions for the new observations, the Johnson & Pilachowski (2010, JP10) measurements, and the combined data sets. Note that the biased sample presented here finds fewer stars with  $[Fe/H] > -1.5$  but more stars with  $[Fe/H] < -2.0$ . The new observations indicate an apparent population of very metal-poor stars that peak near  $[Fe/H] \sim -2.4$ . These stars are near or below the globular cluster metallicity floor found in the Milky Way and other galaxies.

The targets were selected to have minimal overlap with other high resolution spectroscopic studies; however, the present sample does have 8 stars in common with Marino et al. (2011). A comparison between the two studies indicates good agreement with a mean offset in  $[Fe/H]$  of 0.0 dex and a dispersion of 0.13 dex, which is comparable to the mean line-to-line  $[Fe/H]$  dispersion reported in Table 1 for our analysis. We also have 52

<sup>5</sup> We reiterate that the targets have already been selected to have membership probabilities  $> 70\%$ , based on the van Leeuwen et al. (2000) proper motion analysis.

<sup>6</sup> Note that the Anders & Grevesse (1989) solar abundances were used for consistency with Johnson & Pilachowski (2010).

stars in common with the low resolution ( $R \sim 2000$ ) spectroscopic analysis by An et al. (2017) that shows a mean offset, in the sense of the present work minus the literature value, of +0.12 dex and a dispersion of 0.15 dex. We attribute the worse agreement to the order of magnitude lower resolution in the An et al. (2017) data.

The  $[\text{Fe}/\text{H}]$  error values ( $\Delta[\text{Fe}/\text{H}]$ ) provided in Table 1 take into account several factors added in quadrature, including the standard error of the mean  $[\text{Fe}/\text{H}]$  value and uncertainties related to temperature ( $\Delta T_{\text{eff}} = 100$  K), surface gravity ( $\Delta \log(g) = 0.15$  cgs), model atmosphere metallicity ( $\Delta[\text{M}/\text{H}] = 0.15$  dex), and microturbulence ( $\Delta\xi_{\text{mic.}} = 0.13 \text{ km s}^{-1}$ ) errors. However, since we exclusively used Fe I lines the error budget is dominated by the  $T_{\text{eff}}$ ,  $\xi_{\text{mic.}}$ , and measurement uncertainties, which also includes  $\log gf$  and continuum normalization and/or fitting errors. Typical uncertainties are approximately 0.14 dex in  $[\text{Fe}/\text{H}]$ . Since corrections for departures from local thermodynamic equilibrium (LTE) are not available for several of the lines used here, all  $[\text{Fe}/\text{H}]$  measurements assume LTE. Fortunately, calculations from several authors (Bergemann et al. 2012; Lind et al. 2012; Mashonkina et al. 2016) indicate that absolute Fe I non-LTE corrections should be  $\lesssim 0.05$ -0.10 dex in magnitude for the parameter space analyzed here. Relative differences between stars with similar temperatures should be even smaller.

#### 4. RESULTS AND DISCUSSION

As mentioned in §1, one of  $\omega$  Cen's most intriguing properties is its large metallicity spread. Numerous authors have used large sample spectroscopic (Norris & Da Costa 1995; Norris et al. 1996; Suntzeff & Kraft 1996; Villanova et al. 2007; Johnson et al. 2008; Johnson & Pilachowski 2010; Marino et al. 2011; Pancino et al. 2011b,a; Villanova et al. 2014; An et al. 2017; Mucciarelli et al. 2018) and photometric (Lee et al. 1999; Hilker & Richtler 2000; Pancino et al. 2000; Rey et al. 2004; Sollima et al. 2005; Calamida et al. 2009; Bellini et al. 2010; Calamida et al. 2017) surveys to show that the cluster has at least 5-6 populations with unique  $[\text{Fe}/\text{H}]$  values. Peaks in the metallicity distribution function are generally found near  $[\text{Fe}/\text{H}] \sim -1.75$ ,  $-1.50$ ,  $-1.20$ , and  $-0.70$  (see also Figure 3), and tend to cluster on well-defined RGB sequences. Pancino et al. (2011b) claim to find a more metal-poor population, rather than simply a metal-poor tail, near  $[\text{Fe}/\text{H}] \sim -2$ , which suggests that additional minority populations of very metal-poor stars may still be awaiting discovery.

Finding cluster members with  $[\text{Fe}/\text{H}] \lesssim -2.3$  would be important for linking  $\omega$  Cen's formation to a dwarf

galaxy environment because such stars are not expected in globular clusters. A nearly universal globular cluster metallicity floor exists near  $[\text{Fe}/\text{H}] \sim -2.3$  to  $-2.5$  for Local Group galaxies (e.g., Beasley et al. 2019) as well as the Milky Way (e.g., Simpson 2018), and  $\omega$  Cen's retrograde, but confined to the plane (e.g., Majewski et al. 2012), orbit precludes capturing metal-poor stars from the Galactic halo. Therefore, very metal-poor stars found in  $\omega$  Cen today would likely have originated as a field population in the cluster's progenitor system. If  $\omega$  Cen formed in an environment similar to the dwarf galaxies observed today, then knowledge of the cluster's  $[\text{Fe}/\text{H}]$  floor could help place constraints on the metallicity distribution function of its host galaxy.

##### 4.1. Very Metal-poor Stars in $\omega$ Cen

In Figure 3 we compare the biased metallicity distribution function derived here against the relatively unbiased distribution found by Johnson & Pilachowski (2010). The new observations clearly confirm the presence of the dominant metal-poor population near  $[\text{Fe}/\text{H}] \sim -1.7$  and the intermediate metallicity group at  $[\text{Fe}/\text{H}] \sim -1.5$ , and as expected from our selection procedure we find far fewer stars with  $[\text{Fe}/\text{H}] \gtrsim -1.3$ . Figure 4 further shows that our  $[\text{Fe}/\text{H}]$  determinations follow the expected correlation between metallicity and RGB color, and that most of the stars in our sample with  $[\text{Fe}/\text{H}] \gtrsim -1.3$  lie on the AGB or red HB sequences.

We find a possible metal-poor population near  $[\text{Fe}/\text{H}] \sim -2.1$  that appears separate from the dominant group at  $[\text{Fe}/\text{H}] \sim -1.7$  (see also § 4.1.1), and we suspect that these RGB stars are part of the same metal-poor fraction identified by Pancino et al. (2011b) on the SGB. Interestingly, we also find a new population of 11 stars with metallicities below the  $[\text{Fe}/\text{H}] = -2.26$  limit set by Johnson & Pilachowski (2010). These stars represent 2.8% of our sample and span from  $[\text{Fe}/\text{H}] = -2.30$  to  $-2.52$ . Figure 4 further shows that these very metal-poor stars generally fall on the blue edge of the cluster RGB, as expected, but 2-3 of the targets could be AGB or HB stars. The very metal-poor stars identified here are close to the empirically determined globular cluster metallicity floor noted in Beasley et al. (2019).

The existence of a metal-poor tail in  $\omega$  Cen is already a unique trait among iron-complex clusters. The metallicity distribution functions for all iron-complex clusters except  $\omega$  Cen possess a sharp rise at low metallicity, one or more populations at higher metallicity, and occasionally a metal-rich tail. The only other compelling case for a cluster hosting a metal-poor tail or a minor population at low metallicity is Terzan 5, which has a dominant population near  $[\text{Fe}/\text{H}] \sim -0.3$ , a secondary

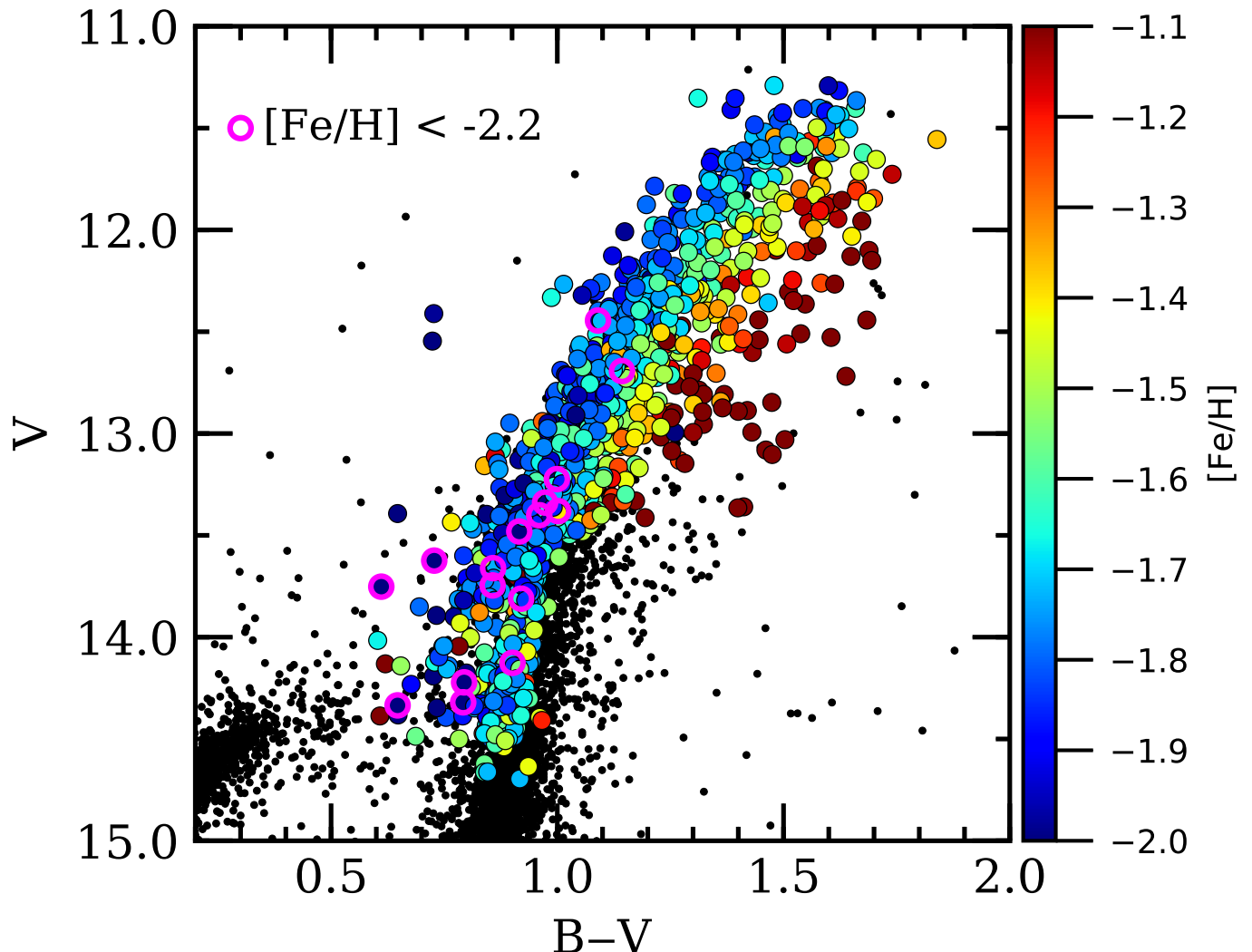


**Figure 4.** An  $\omega$  Cen V versus B–V color-magnitude diagram is shown using the photometric data from van Leeuwen et al. (2000, black circles). The large filled circles are color coded by  $[Fe/H]$  using spectroscopic abundances from Johnson & Pilachowski (2010) and the present work. The large open magenta circles indicate stars in either study with  $[Fe/H] < -2.2$  dex. Note that the color gradient is saturated at  $[Fe/H] = -2$  dex on the metal-poor end and  $[Fe/H] = -1.1$  dex on the metal-rich end.

population at  $[Fe/H] \sim +0.25$ , and a minority ( $\lesssim 6\%$ ) metal-poor group at  $[Fe/H] \sim -0.8$  (Origlia et al. 2013; Massari et al. 2014). However, the various Terzan 5 subpopulations do not possess the complex light element variations observed in  $\omega$  Cen.

Other than metallicity, do the most metal-poor stars in  $\omega$  Cen possess any unusual properties? Figure 5 compares the radial and spatial distributions, radial velocities, and Gaia DR2 proper motions for the stars analyzed in the present study. Visual inspection of the two left panels in Figure 5 indicate that: (1) stars with  $[Fe/H] < -2$  span a broad range in right ascension but only populate a narrow range in declination and (2) the most metal-poor stars may be very centrally concentrated. First addressing the spatial distribution, we note that the dispersion in declination for stars with  $[Fe/H] >$

$-2$  is 0.128 degrees while the dispersions for stars with  $-2.25 \leq [Fe/H] \leq -2$  and  $[Fe/H] < -2.25$  are 0.023 and 0.029 degrees, respectively. Similarly, two-sided Kolmogorov-Smirnov (KS) tests comparing the declination distributions of all stars versus first those with  $[Fe/H] < -2$  and then those with  $[Fe/H] < -2.25$  returned  $p$ -values<sup>7</sup> of 0.002 and 0.095, respectively. From these data we can conclude that there is marginal evidence indicating that the most metal-poor  $\omega$  Cen stars may be confined to a more narrow plane than the majority of cluster stars. However, a larger sample size is required to draw any strong conclusions.

<sup>7</sup> We adopt the common convention that a  $p$ -value  $< 0.05$  is sufficient to reject the null hypothesis.

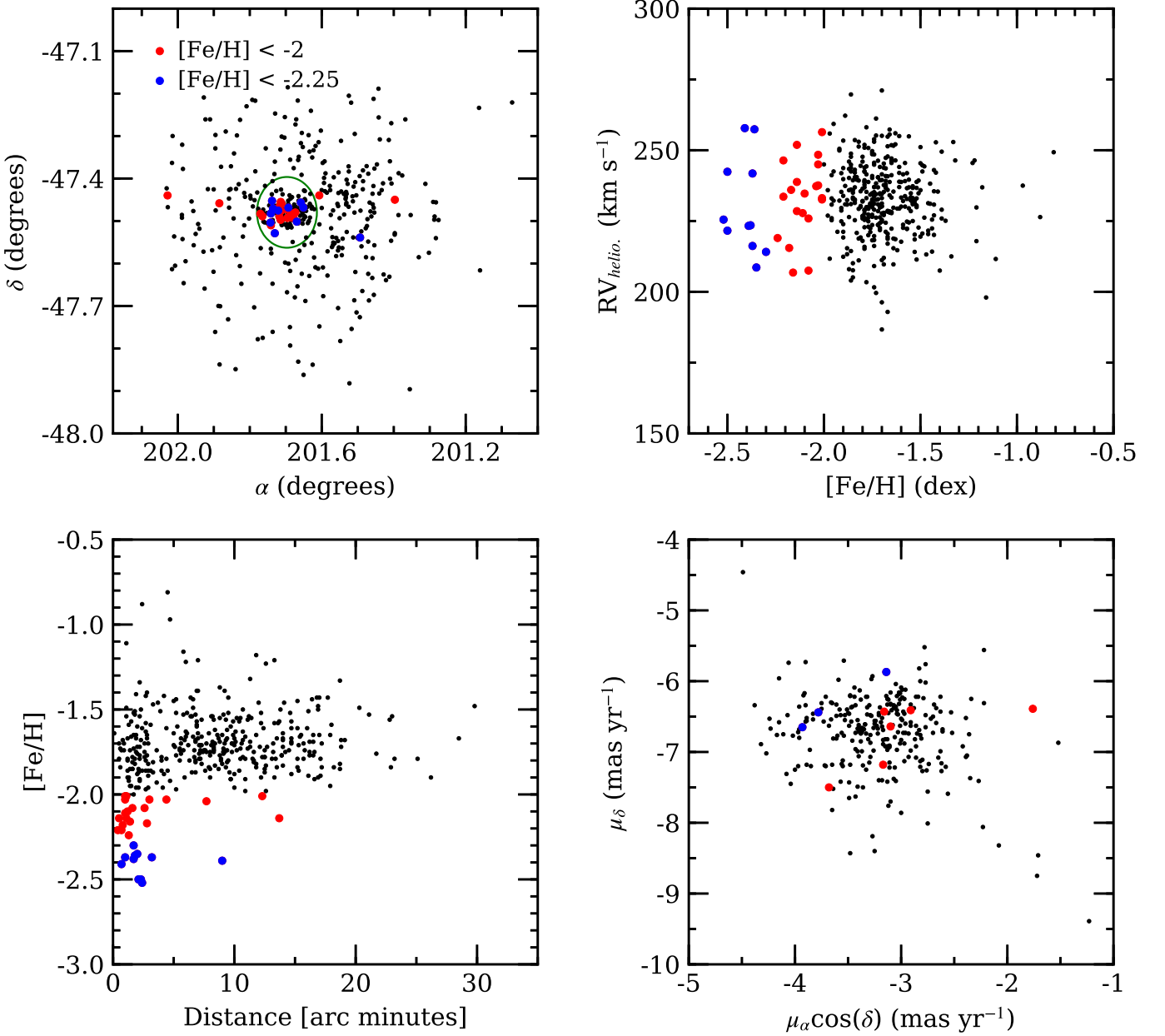


**Figure 5.** *Top left:* the black circles indicate the J2000 sky coordinates of all  $\omega$  Cen giants observed for the present study while the large red circles indicate stars with  $[\text{Fe}/\text{H}] < -2$  dex. The most metal-poor stars with  $[\text{Fe}/\text{H}] < -2.25$  are indicated as large blue circles. The green ellipse illustrates the cluster's approximate half-light radius ( $5'$ ). Although nearly all of the metal-poor stars identified in the present work reside within the cluster half-light radius, the stars farther out are only found within a narrow declination range. *Top right:* heliocentric radial velocities are plotted as a function of  $[\text{Fe}/\text{H}]$  using the same symbols as in the left panel. The metal-poor stars do not exhibit any obvious radial velocity peculiarities. *Bottom left:*  $[\text{Fe}/\text{H}]$  is plotted as a function of radial distance from the cluster center. Note that the stars with  $[\text{Fe}/\text{H}] < -2$  appear to be centrally concentrated. *Bottom right:* Gaia DR2 proper motion values are plotted using the same symbols as the left panel. We do not find the metal-poor stars to exhibit any systematic proper motion differences relative to the higher metallicity stars.

Regarding the radial distributions, Figure 5 shows that nearly all of the stars with  $[\text{Fe}/\text{H}] < -2$  are projected within  $12'$  of the cluster core and 84% are within  $3'$ . Similarly, all of the stars with  $[\text{Fe}/\text{H}] < -2.25$  are within  $10'$  and 81% are inside of  $3'$ . These results match previous observations by Johnson & Pilachowski (2010)

who noted that 88% of the stars in their sample with  $[\text{Fe}/\text{H}] < -2$  were found within  $5'$  of the cluster core. The combination of the present work with the larger sample of Johnson & Pilachowski (2010) hints that the most metal-poor stars in  $\omega$  Cen may be mostly confined to within a half-light radius ( $5'$ ). A two-sided KS test

comparing the radial distributions of stars with  $[Fe/H] > -2$  against those with  $[Fe/H] < -2$  returned a  $p$ -value of  $2.91 \times 10^{-10}$  while a similar test comparing the radial distributions of stars with  $[Fe/H] > -2$  and  $[Fe/H] < -2.25$  returned a  $p$ -value of  $8.66 \times 10^{-5}$ . The extremely low  $p$ -values indicate a low probability that stars with  $[Fe/H] < -2$  follow the same radial distribution as their higher metallicity counterparts. We did not detect any further differences between the most metal-poor stars and any other populations when examining radial velocity or proper motion distributions; however, larger sample sizes are required to draw any firm conclusions.

#### 4.1.1. Do the Very Metal-poor Stars Form Distinct Populations?

An important question when examining the metallicity distribution function of  $\omega$  Cen is whether the stars with  $[Fe/H] < -2$  form distinct populations or simply an extended tail. As noted previously, the binned distributions shown in Figure 3 indicate possible “peaks” near  $[Fe/H] \sim -2.1$  and  $-2.4$ , but the sample sizes are small. To help determine whether the most metal-poor stars are separate populations, we utilize the Gaussian mixture model (GMM) method described in Ashman et al. (1994) via the implementation outlined in Muratov & Gnedin (2010) to examine: (1) if the peak near  $[Fe/H] = -2.1$  is distinct from the dominant population near  $[Fe/H] = -1.7$ ; and (2) if the groups at  $[Fe/H] = -2.1$  and  $-2.4$  are separate or part of a broad unimodal population.

The modality analysis described in Muratov & Gnedin (2010) includes an algorithm for a likelihood ratio test that determines whether the sum of two Gaussian profiles provides an improvement over fitting a unimodal Gaussian distribution. Note that we have adopted the homoschedastic case (equal variance) for all GMM tests, which is a reasonable assumption if the  $[Fe/H]$  spread within each population is dominated by equivalent measurement errors. Since the likelihood ratio test assumes Gaussian distributions, Ashman et al. (1994) and Muratov & Gnedin (2010) also include a dimensionless mode separation statistic defined as,

$$D \equiv \frac{|\mu_1 - \mu_2|}{\sqrt{(\sigma_1^2 + \sigma_2^2)/2}}, \quad (3)$$

where  $D > 2$  is required for a clear separation between two modes when the mean ( $\mu$ ) and dispersion ( $\sigma$ ) values for two populations are known. Muratov & Gnedin (2010) also note that a negative kurtosis is a “necessary but not sufficient condition of bimodality”. However, since the number of very metal-poor stars in our sample is small, especially relative to the dominant population

at  $[Fe/H] \sim -1.7$ , we do not include kurtosis measurements here.

For the first case listed above, we compiled a list of stars with  $-2.25 \leq [Fe/H] \leq -1.60$  from Table 1 and ran the Muratov & Gnedin (2010) algorithm to determine whether a bimodal distribution was an improvement over fitting a single Gaussian profile. The Muratov & Gnedin (2010) test found that the data were better fit assuming two Gaussian distributions with means of  $[Fe/H] = -2.07$  and  $-1.76$  ( $\sigma = 0.09$  dex) over a single Gaussian with a mean of  $[Fe/H] = -1.78$  and a larger dispersion ( $\sigma = 0.11$  dex) at more than the 99.9% level. A bootstrap analysis yielded a separation statistic of  $D = 3.38 \pm 0.41$ , which provides a high level of confidence that the peak at  $[Fe/H] = -2.07$  represents a legitimate population rather than a metal-poor tail for the  $[Fe/H] = -1.76$  group.

For the second case, we examined the  $[Fe/H]$  distribution for all stars in Table 1 with  $[Fe/H] < -2$  to determine if these objects form two narrow populations or one broad distribution. We determined that a unimodal distribution was ruled out at the more than 99.6% level, and that two populations were preferred having means of  $[Fe/H] = -2.4$  and  $-2.1$  with dispersions of 0.07 dex. The bootstrap mode separation statistic was calculated to be  $D = 4.37 \pm 0.8$ , which suggests that if two populations are present below  $[Fe/H] = -2$  then their mean metallicities are well-separated.

#### 4.2. Origin of the Very Metal-poor Stars

If the stars in  $\omega$  Cen with  $[Fe/H] < -2$ , and especially those with  $[Fe/H] < -2.25$ , are truly distinct from the other cluster populations, then their presence may reveal important details about the cluster’s early formation history. The available evidence suggests several possible origins for  $\omega$  Cen’s very metal-poor stars, including: (1) early star formation in the unenriched primordial cloud, (2) the capture of surrounding field stars, assuming the cluster formed in a dwarf galaxy, or (3) an early merger between  $\omega$  Cen and a pre-existing but metal-poor sub-structure.

##### 4.2.1. Early Star Formation

The primordial cloud scenario is the most straightforward, and would imply that the very metal-poor stars trace the original composition of the molecular cloud from which  $\omega$  Cen formed. Data from Johnson & Pilachowski (2010) and Pancino et al. (2011b) indicate that stars with  $[Fe/H] < -2$  may have reduced light element abundance variations compared to their more metal-rich counterparts, which might be consistent with an early proto-cluster environment that

had not yet been polluted by sources such as intermediate mass AGB stars. However, if  $\omega$  Cen actually has two populations of very metal-poor stars at  $[Fe/H] \sim -2.1$  and  $-2.4$ , as is suggested in Figure 3 and § 4.1.1, then the cluster could have experienced at least two early small bursts of star formation. Detailed light and heavy element abundance measurements for the  $[Fe/H] \sim -2.4$  stars identified here would help determine if the two groups are chemically similar.

Examining the published metallicity distribution functions of other iron-complex clusters, we note that aside from Terzan 5 only M 54 appears as a possible candidate to host a metal-poor tail. However, the most metal-poor stars in this system were clearly polluted, as evidenced by their large (anti-)correlated light element abundance variations (e.g., Carretta et al. 2010b), and would therefore not represent a pristine population. Similarly, we note that monometallic clusters have significant populations of “primordial” stars that appear to be almost entirely polluted by supernovae, but these stars do not have different  $[Fe/H]$  abundances from other cluster members. Therefore, either  $\omega$  Cen and Terzan 5 were unique in their ability to retain stars that formed before the first major star formation and light element enrichment episode, or their very metal-poor populations have a different origin.

#### 4.2.2. Captured Field Stars

The captured field star scenario is intriguing because it could provide a direct link between present day iron-complex clusters and dwarf galaxies. However, if  $\omega$  Cen formed within a dwarf galaxy should we expect such a system to host many very metal-poor stars? We can draw two reasonable conclusions based on  $\omega$  Cen’s properties alone. First,  $\omega$  Cen’s mass of  $\sim 4 \times 10^6 M_{\odot}$  (D’Souza & Rix 2013) means that its host galaxy must have had a mass of at least  $10^7$ - $10^8 M_{\odot}$  (see also Bekki & Tsujimoto 2019; Myeong et al. 2019). Second, the dwarf galaxy mass-metallicity relation from Kirby et al. (2013) implies that the cluster’s host galaxy likely had a mean metallicity of at least  $[Fe/H] = -1.5$  to  $-1$ . A comparatively high metallicity field star population is qualitatively in agreement with the M 54/Sagittarius system where the mean metallicity of M 54 ( $[Fe/H] \sim -1.6$ ) is several times lower than the Sagittarius field (e.g., Carretta et al. 2010b). Nevertheless, dwarf galaxies tend to have long metal-poor tails (e.g., Leaman et al. 2013), and even cases such as Sagittarius that have a majority of stars with  $[Fe/H] > -1$  contain stars with metallicities as low as  $-2.2$  (Chiti & Frebel 2019). It therefore remains plausible that  $\omega$  Cen could

have existed in an environment that also hosted very metal-poor field stars.

The ability of  $\omega$  Cen to capture very metal-poor stars might depend not only on the metallicity distribution of its host galaxy, but also the cluster’s typical galactocentric radius and the galaxy’s star formation history before tidal disruption. Existing Local Group dwarf galaxies generally exhibit negative metallicity gradients such that the mean metallicity decreases at larger galactocentric distances (e.g., Harbeck et al. 2001; Battaglia et al. 2006; Faria et al. 2007; Carrera et al. 2008; Kirby et al. 2011; Kacharov et al. 2017). If  $\omega$  Cen resided in the core of its host galaxy and a significant fraction of the cluster’s metal-poor stars were captured, then  $\omega$  Cen’s host galaxy might have had an unusually metal-poor core. Alternatively, the cluster’s host galaxy could have had an inverted metallicity gradient (e.g., Wang et al. 2019).

Although  $\omega$  Cen is the most massive cluster associated with the Sequoia (Myeong et al. 2019) or Gaia-Enceladus (Massari et al. 2019) merger events, that does not necessarily mean the cluster always (or ever) resided in its host galaxy’s center. For example, M 54 is the most massive cluster associated with Sagittarius and presently lies near the galaxy’s core, but the cluster could have formed outside the galaxy nucleus and drifted to the center via dynamical friction (e.g., Bellazzini et al. 2008). Furthermore, the Fornax dwarf galaxy has five globular clusters (Shapley 1938; Hodge 1961) and all except one (Fornax 4), including the most massive and metal-poor cluster Fornax 3 (de Boer & Fraser 2016), reside well outside the core radius. One might expect that if  $\omega$  Cen were in a configuration similar to that of Fornax 3 it would have a reasonable chance of capturing metal-poor field stars.

Regardless of where  $\omega$  Cen may have resided within a host galaxy, it could not capture metal-poor field stars unless they were present in significant numbers. Combining the present sample with Johnson & Pilachowski (2010), 3.9% of stars in  $\omega$  Cen have  $[Fe/H] < -2$  and about 1% have  $[Fe/H] < -2.3$ . For comparison, Starkenburg et al. (2010) showed that the fractions of stars with  $[Fe/H] < -2.5$  were 1%, 8%, 8%, and 33% for the Fornax, Carina, Sculptor, and Sextans Local Group dwarf galaxies, respectively.

These observations suggest that  $\omega$  Cen’s host galaxy probably had a higher fraction of metal-poor stars than Fornax, especially if all  $\omega$  Cen stars with  $[Fe/H] < -2$  were captured. In contrast, the metallicity distribution of Sextans may be too metal-poor since we did not find any stars with  $[Fe/H] \lesssim -2.5$ . However, we investigated the color-color distribution of stars in  $\omega$  Cen using recent Sky Mapper (Wolf et al. 2018) photometry and found a

small number of stars that may have  $[Fe/H] < -2.5$  to  $-3$ . A galaxy like Sculptor, but with the globular cluster specific frequency of Fornax, may serve as a reasonable model of  $\omega$  Cen's host galaxy since it has: (1) a mean  $[Fe/H]$  value that is higher than  $\omega$  Cen, (2) a small but significant population of field stars down to  $[Fe/H] \sim -3.0$ , and (3) few stars with  $[Fe/H] \gtrsim -1$  (e.g., Kirby et al. 2009; Starkenburg et al. 2010). The small ( $\sim 10 \text{ km s}^{-1}$ ) velocity dispersion of Fornax globular clusters and field stars (e.g., Hendricks et al. 2014) would also provide a model that is conducive to tidal capture, but it remains to be seen whether such a scenario could be reconciled with the observed central concentration of very metal-poor stars in  $\omega$  Cen.

#### 4.2.3. Merging Sub-clumps

Globular clusters are likely the end results of complicated hierarchical merging processes (e.g., Bonnell et al. 2003; Smilgys & Bonnell 2017), and in this sense the rarity of very metal-poor stars among iron-complex clusters could be a result of this stochastic process. Sub-clump and cluster-cluster mergers have been invoked to explain several globular cluster properties in the past (e.g., van den Bergh 1996; Lee et al. 1999; Carretta et al. 2010c; Bekki & Tsujimoto 2019), and we posit that such a model may explain the existence of the metal-poor populations in  $\omega$  Cen, and possibly Terzan 5, as well.

In this model, the early  $\omega$  Cen environment would have been subject to intense star formation and molecular cloud and/or cluster mergers. As a result, the main  $\omega$  Cen structure could have coalesced with a sub-structure that was either in the process of forming or already fully formed, but that had a very low metallicity and not enough time to experience significant light element self-enrichment. Since the most metal-poor stars in  $\omega$  Cen do not reach below the empirical globular cluster limit of  $[Fe/H] \sim -2.5$  and Figure 3 hints at two different populations with  $[Fe/H] < -2$  rather than a continuous metal-poor tail, a merging sub-structure scenario may be favored over a field star capture model. If the merging sub-structures were also relatively massive, they might naturally fall to the cluster center and help explain the central concentration of stars with  $[Fe/H] < -2$  shown in Figure 5.

Although the stars with  $[Fe/H] < -2$  constitute only a small fraction of  $\omega$  Cen's mass, we did not detect any unusual kinematic properties for these populations. As a result, the sub-clump merger origin for very metal-

poor stars may only be plausible if their initial kinematic signature was erased by dynamical evolution or was very similar to the existing  $\omega$  Cen proto-cluster.

## 5. SUMMARY

We present  $[Fe/H]$  measurements, based on high resolution M2FS spectra, for 395 giants in the massive globular cluster  $\omega$  Cen. The targets were chosen to reside on the blue half of the RGB in an effort to find the most metal-poor stars in the cluster. Previous attempts identified a metal-poor population with  $[Fe/H] \sim -2.1$  but failed to find any stars with  $[Fe/H] \lesssim -2.25$ . However, we have identified 11 new stars with metallicities ranging from  $[Fe/H] = -2.30$  to  $-2.52$ , which places these stars near the empirical globular cluster metallicity floor observed among the Milky Way and other Local Group galaxies.

The metal-poor stars identified here and in previous studies appear to be very centrally concentrated, and may also be confined to a narrow declination plane. However, these stars do not appear to exhibit any peculiar kinematic properties that distinguish them from the more metal-rich populations in  $\omega$  Cen. We examine three possible scenarios in which  $\omega$  Cen could form or capture stars that are significantly more metal-poor than its dominant population at  $[Fe/H] \sim -1.7$ . Specifically, the very metal-poor stars could: (1) trace very early star formation in the cluster, (2) have originated as captured field stars from  $\omega$  Cen's original host galaxy, or (3) represent an early merger event between  $\omega$  Cen and metal-poor sub-clumps. Although none of these scenarios is clearly favored, the merging sub-clump model may have the greatest chance for describing the paucity of very metal-poor stars in other clusters, the possibly reduced light element spread for stars with  $[Fe/H] < -2$ , and the observed central concentration of these populations.

## ACKNOWLEDGMENTS

CIJ and AKD gratefully acknowledge support from the Scholarly Studies Program of the Smithsonian Institution. EWO, MGW, and MM acknowledge support from the National Science Foundation under grants AST-1815767, AST-1813881, and AST-1815403.

*Facilities:* Magellan(M2FS)

## REFERENCES

- Afsar, M., Sneden, C., Frebel, A., et al. 2016, ApJ, 819, 103, doi: [10.3847/0004-637X/819/2/103](https://doi.org/10.3847/0004-637X/819/2/103)
- Alonso, A., Arribas, S., & Martínez-Roger, C. 1999, A&AS, 140, 261, doi: [10.1051/aas:1999521](https://doi.org/10.1051/aas:1999521)

- An, D., Lee, Y. S., In Jung, J., et al. 2017, AJ, 154, 150, doi: [10.3847/1538-3881/aa8364](https://doi.org/10.3847/1538-3881/aa8364)
- Anders, E., & Grevesse, N. 1989, GeoCoA, 53, 197, doi: [10.1016/0016-7037\(89\)90286-X](https://doi.org/10.1016/0016-7037(89)90286-X)
- Ashman, K. M., Bird, C. M., & Zepf, S. E. 1994, AJ, 108, 2348, doi: [10.1086/117248](https://doi.org/10.1086/117248)
- Bailin, J. 2019, arXiv e-prints, arXiv:1909.11731. <https://arxiv.org/abs/1909.11731>
- Battaglia, G., Tolstoy, E., Helmi, A., et al. 2006, A&A, 459, 423, doi: [10.1051/0004-6361:20065720](https://doi.org/10.1051/0004-6361:20065720)
- Beasley, M. A., Leaman, R., Gallart, C., et al. 2019, MNRAS, 487, 1986, doi: [10.1093/mnras/stz1349](https://doi.org/10.1093/mnras/stz1349)
- Bekki, K., & Freeman, K. C. 2003, MNRAS, 346, L11, doi: [10.1046/j.1365-2966.2003.07275.x](https://doi.org/10.1046/j.1365-2966.2003.07275.x)
- Bekki, K., & Tsujimoto, T. 2019, arXiv e-prints, arXiv:1909.11295. <https://arxiv.org/abs/1909.11295>
- Bellazzini, M., Ibata, R. A., Chapman, S. C., et al. 2008, AJ, 136, 1147, doi: [10.1088/0004-6256/136/3/1147](https://doi.org/10.1088/0004-6256/136/3/1147)
- Bellini, A., Bedin, L. R., Piotto, G., et al. 2010, AJ, 140, 631, doi: [10.1088/0004-6256/140/2/631](https://doi.org/10.1088/0004-6256/140/2/631)
- Bellini, A., Milone, A. P., Anderson, J., et al. 2017, ApJ, 844, 164, doi: [10.3847/1538-4357/aa7b7e](https://doi.org/10.3847/1538-4357/aa7b7e)
- Bergemann, M., Lind, K., Collet, R., Magic, Z., & Asplund, M. 2012, MNRAS, 427, 27, doi: [10.1111/j.1365-2966.2012.21687.x](https://doi.org/10.1111/j.1365-2966.2012.21687.x)
- Bonnell, I. A., Bate, M. R., & Vine, S. G. 2003, MNRAS, 343, 413, doi: [10.1046/j.1365-8711.2003.06687.x](https://doi.org/10.1046/j.1365-8711.2003.06687.x)
- Bono, G., Iannicola, G., Braga, V. F., et al. 2019, ApJ, 870, 115, doi: [10.3847/1538-4357/aaf23f](https://doi.org/10.3847/1538-4357/aaf23f)
- Calamida, A., Stetson, P. B., Bono, G., et al. 2005, ApJL, 634, L69, doi: [10.1086/498691](https://doi.org/10.1086/498691)
- Calamida, A., Bono, G., Stetson, P. B., et al. 2009, ApJ, 706, 1277, doi: [10.1088/0004-637X/706/2/1277](https://doi.org/10.1088/0004-637X/706/2/1277)
- Calamida, A., Strampelli, G., Rest, A., et al. 2017, AJ, 153, 175, doi: [10.3847/1538-3881/aa6397](https://doi.org/10.3847/1538-3881/aa6397)
- Carrera, R., Gallart, C., Aparicio, A., et al. 2008, AJ, 136, 1039, doi: [10.1088/0004-6256/136/3/1039](https://doi.org/10.1088/0004-6256/136/3/1039)
- Carretta, E., Bragaglia, A., Gratton, R., D’Orazi, V., & Lucatello, S. 2009, A&A, 508, 695, doi: [10.1051/0004-6361/200913003](https://doi.org/10.1051/0004-6361/200913003)
- Carretta, E., Bragaglia, A., Gratton, R. G., et al. 2010a, ApJL, 714, L7, doi: [10.1088/2041-8205/714/1/L7](https://doi.org/10.1088/2041-8205/714/1/L7)
- . 2010b, A&A, 520, A95, doi: [10.1051/0004-6361/201014924](https://doi.org/10.1051/0004-6361/201014924)
- Carretta, E., Gratton, R. G., Lucatello, S., et al. 2010c, ApJL, 722, L1, doi: [10.1088/2041-8205/722/1/L1](https://doi.org/10.1088/2041-8205/722/1/L1)
- Castelli, F., & Kurucz, R. L. 2003, in IAU Symposium, Vol. 210, Modelling of Stellar Atmospheres, ed. N. Piskunov, W. W. Weiss, & D. F. Gray, A20. <https://arxiv.org/abs/astro-ph/0405087>
- Chiti, A., & Frebel, A. 2019, ApJ, 875, 112, doi: [10.3847/1538-4357/ab0f9f](https://doi.org/10.3847/1538-4357/ab0f9f)
- Da Costa, G. S. 2016, in IAU Symposium, Vol. 317, The General Assembly of Galaxy Halos: Structure, Origin and Evolution, ed. A. Bragaglia, M. Arnaboldi, M. Rejkuba, & D. Romano, 110–115, doi: [10.1017/S174392131500678X](https://doi.org/10.1017/S174392131500678X)
- D’Antona, F., D’Ercole, A., Marino, A. F., et al. 2011, ApJ, 736, 5, doi: [10.1088/0004-637X/736/1/5](https://doi.org/10.1088/0004-637X/736/1/5)
- de Boer, T. J. L., & Fraser, M. 2016, A&A, 590, A35, doi: [10.1051/0004-6361/201527580](https://doi.org/10.1051/0004-6361/201527580)
- Dinescu, D. I., Girard, T. M., & van Altena, W. F. 1999, AJ, 117, 1792, doi: [10.1086/300807](https://doi.org/10.1086/300807)
- D’Souza, R., & Rix, H.-W. 2013, MNRAS, 429, 1887, doi: [10.1093/mnras/sts426](https://doi.org/10.1093/mnras/sts426)
- Faria, D., Feltzing, S., Lundström, I., et al. 2007, A&A, 465, 357, doi: [10.1051/0004-6361:20065244](https://doi.org/10.1051/0004-6361:20065244)
- Frebel, A., Chiti, A., Ji, A. P., Jacobson, H. R., & Placco, V. M. 2015, ApJL, 810, L27, doi: [10.1088/2041-8205/810/2/L27](https://doi.org/10.1088/2041-8205/810/2/L27)
- Georgiev, I. Y., Hilker, M., Puzia, T. H., Goudfrooij, P., & Baumgardt, H. 2009, MNRAS, 396, 1075, doi: [10.1111/j.1365-2966.2009.14776.x](https://doi.org/10.1111/j.1365-2966.2009.14776.x)
- Harbeck, D., Grebel, E. K., Holtzman, J., et al. 2001, AJ, 122, 3092, doi: [10.1086/324232](https://doi.org/10.1086/324232)
- Helmi, A., Babusiaux, C., Koppelman, H. H., et al. 2018, Nature, 563, 85, doi: [10.1038/s41586-018-0625-x](https://doi.org/10.1038/s41586-018-0625-x)
- Hendricks, B., Koch, A., Walker, M., et al. 2014, A&A, 572, A82, doi: [10.1051/0004-6361/201424645](https://doi.org/10.1051/0004-6361/201424645)
- Hilker, M., & Richtler, T. 2000, A&A, 362, 895. <https://arxiv.org/abs/astro-ph/0008500>
- Hodge, P. W. 1961, AJ, 66, 83, doi: [10.1086/108378](https://doi.org/10.1086/108378)
- Ibata, R. A., Bellazzini, M., Malhan, K., Martin, N., & Bianchini, P. 2019, Nature Astronomy, 3, 667, doi: [10.1038/s41550-019-0751-x](https://doi.org/10.1038/s41550-019-0751-x)
- Johnson, C. I., Caldwell, N., Rich, R. M., et al. 2017, ApJ, 836, 168, doi: [10.3847/1538-4357/836/2/168](https://doi.org/10.3847/1538-4357/836/2/168)
- Johnson, C. I., Kraft, R. P., Pilachowski, C. A., et al. 2005, PASP, 117, 1308, doi: [10.1086/497435](https://doi.org/10.1086/497435)
- Johnson, C. I., & Pilachowski, C. A. 2010, ApJ, 722, 1373, doi: [10.1088/0004-637X/722/2/1373](https://doi.org/10.1088/0004-637X/722/2/1373)
- Johnson, C. I., Pilachowski, C. A., Simmerer, J., & Schwenk, D. 2008, ApJ, 681, 1505, doi: [10.1086/588634](https://doi.org/10.1086/588634)
- Johnson, C. I., Rich, R. M., Pilachowski, C. A., et al. 2015a, AJ, 150, 63, doi: [10.1088/0004-6256/150/2/63](https://doi.org/10.1088/0004-6256/150/2/63)
- Johnson, C. I., McDonald, I., Pilachowski, C. A., et al. 2015b, AJ, 149, 71, doi: [10.1088/0004-6256/149/2/71](https://doi.org/10.1088/0004-6256/149/2/71)
- Kacharov, N., Battaglia, G., Rejkuba, M., et al. 2017, MNRAS, 466, 2006, doi: [10.1093/mnras/stw3188](https://doi.org/10.1093/mnras/stw3188)
- Kirby, E. N., Cohen, J. G., Guhathakurta, P., et al. 2013, ApJ, 779, 102, doi: [10.1088/0004-637X/779/2/102](https://doi.org/10.1088/0004-637X/779/2/102)

- Kirby, E. N., Guhathakurta, P., Bolte, M., Sneden, C., & Geha, M. C. 2009, ApJ, 705, 328, doi: [10.1088/0004-637X/705/1/328](https://doi.org/10.1088/0004-637X/705/1/328)
- Kirby, E. N., Lanfranchi, G. A., Simon, J. D., Cohen, J. G., & Guhathakurta, P. 2011, ApJ, 727, 78, doi: [10.1088/0004-637X/727/2/78](https://doi.org/10.1088/0004-637X/727/2/78)
- Kurtz, M. J., & Mink, D. J. 1998, PASP, 110, 934, doi: [10.1086/316207](https://doi.org/10.1086/316207)
- Leaman, R., Venn, K. A., Brooks, A. M., et al. 2013, ApJ, 767, 131, doi: [10.1088/0004-637X/767/2/131](https://doi.org/10.1088/0004-637X/767/2/131)
- Lee, Y. W., Joo, J. M., Sohn, Y. J., et al. 1999, Nature, 402, 55, doi: [10.1038/46985](https://doi.org/10.1038/46985)
- Lind, K., Bergemann, M., & Asplund, M. 2012, MNRAS, 427, 50, doi: [10.1111/j.1365-2966.2012.21686.x](https://doi.org/10.1111/j.1365-2966.2012.21686.x)
- Mackey, A. D., & van den Bergh, S. 2005, MNRAS, 360, 631, doi: [10.1111/j.1365-2966.2005.09080.x](https://doi.org/10.1111/j.1365-2966.2005.09080.x)
- Magurno, D., Sneden, C., Bono, G., et al. 2019, ApJ, 881, 104, doi: [10.3847/1538-4357/ab2e76](https://doi.org/10.3847/1538-4357/ab2e76)
- Majewski, S. R., Nidever, D. L., Smith, V. V., et al. 2012, ApJL, 747, L37, doi: [10.1088/2041-8205/747/2/L37](https://doi.org/10.1088/2041-8205/747/2/L37)
- Marino, A. F., Milone, A. P., Piotto, G., et al. 2011, ApJ, 731, 64, doi: [10.1088/0004-637X/731/1/64](https://doi.org/10.1088/0004-637X/731/1/64)
- Marino, A. F., Milone, A. P., Karakas, A. I., et al. 2015, MNRAS, 450, 815, doi: [10.1093/mnras/stv420](https://doi.org/10.1093/mnras/stv420)
- Mashonkina, L. I., Sitnova, T. N., & Pakhomov, Y. V. 2016, Astronomy Letters, 42, 606, doi: [10.1134/S1063773716080028](https://doi.org/10.1134/S1063773716080028)
- Massari, D., Koppelman, H. H., & Helmi, A. 2019, A&A, 630, L4, doi: [10.1051/0004-6361/201936135](https://doi.org/10.1051/0004-6361/201936135)
- Massari, D., Mucciarelli, A., Ferraro, F. R., et al. 2014, ApJ, 795, 22, doi: [10.1088/0004-637X/795/1/22](https://doi.org/10.1088/0004-637X/795/1/22)
- Mateo, M., Bailey, J. I., Crane, J., et al. 2012, in Society of Photo-Optical Instrumentation Engineers (SPIE) Conference Series, Vol. 8446, Proc. SPIE, 84464Y, doi: [10.1117/12.926448](https://doi.org/10.1117/12.926448)
- McCall, M. L. 2004, AJ, 128, 2144, doi: [10.1086/424933](https://doi.org/10.1086/424933)
- McDonald, I., Johnson, C. I., & Zijlstra, A. A. 2011, MNRAS, 416, L6, doi: [10.1111/j.1745-3933.2011.01086.x](https://doi.org/10.1111/j.1745-3933.2011.01086.x)
- McDonald, I., van Loon, J. T., Decin, L., et al. 2009, MNRAS, 394, 831, doi: [10.1111/j.1365-2966.2008.14370.x](https://doi.org/10.1111/j.1365-2966.2008.14370.x)
- Milone, A. P., Piotto, G., Renzini, A., et al. 2017, MNRAS, 464, 3636, doi: [10.1093/mnras/stw2531](https://doi.org/10.1093/mnras/stw2531)
- Mucciarelli, A., Salaris, M., Monaco, L., et al. 2018, A&A, 618, A134, doi: [10.1051/0004-6361/201833457](https://doi.org/10.1051/0004-6361/201833457)
- Muratov, A. L., & Gnedin, O. Y. 2010, ApJ, 718, 1266, doi: [10.1088/0004-637X/718/2/1266](https://doi.org/10.1088/0004-637X/718/2/1266)
- Myeong, G. C., Vasiliev, E., Iorio, G., Evans, N. W., & Belokurov, V. 2019, MNRAS, 488, 1235, doi: [10.1093/mnras/stz1770](https://doi.org/10.1093/mnras/stz1770)
- Norris, J. E., & Da Costa, G. S. 1995, ApJ, 447, 680, doi: [10.1086/175909](https://doi.org/10.1086/175909)
- Norris, J. E., Freeman, K. C., & Mighell, K. J. 1996, ApJ, 462, 241, doi: [10.1086/177145](https://doi.org/10.1086/177145)
- Origlia, L., Massari, D., Rich, R. M., et al. 2013, ApJL, 779, L5, doi: [10.1088/2041-8205/779/1/L5](https://doi.org/10.1088/2041-8205/779/1/L5)
- Pancino, E., Ferraro, F. R., Bellazzini, M., Piotto, G., & Zoccali, M. 2000, ApJL, 534, L83, doi: [10.1086/312658](https://doi.org/10.1086/312658)
- Pancino, E., Mucciarelli, A., Bonifacio, P., Monaco, L., & Sbordone, L. 2011a, A&A, 534, A53, doi: [10.1051/0004-6361/201117378](https://doi.org/10.1051/0004-6361/201117378)
- Pancino, E., Mucciarelli, A., Sbordone, L., et al. 2011b, A&A, 527, A18, doi: [10.1051/0004-6361/201016024](https://doi.org/10.1051/0004-6361/201016024)
- Reijns, R. A., Seitzer, P., Arnold, R., et al. 2006, A&A, 445, 503, doi: [10.1051/0004-6361:20053059](https://doi.org/10.1051/0004-6361:20053059)
- Rey, S.-C., Lee, Y.-W., Ree, C. H., et al. 2004, AJ, 127, 958, doi: [10.1086/380942](https://doi.org/10.1086/380942)
- Ryabchikova, T., Piskunov, N., Kurucz, R. L., et al. 2015, PhysS, 90, 054005, doi: [10.1088/0031-8949/90/5/054005](https://doi.org/10.1088/0031-8949/90/5/054005)
- Shapley, H. 1938, Nature, 142, 715, doi: [10.1038/142715b0](https://doi.org/10.1038/142715b0)
- Simpson, J. D. 2018, MNRAS, 477, 4565, doi: [10.1093/mnras/sty847](https://doi.org/10.1093/mnras/sty847)
- Simpson, J. D., Martell, S. L., Da Costa, G., et al. 2019, arXiv e-prints, arXiv:1911.01548, <https://arxiv.org/abs/1911.01548>
- Skrutskie, M. F., Cutri, R. M., Stiening, R., et al. 2006, AJ, 131, 1163, doi: [10.1086/498708](https://doi.org/10.1086/498708)
- Smilgys, R., & Bonnell, I. A. 2017, MNRAS, 472, 4982, doi: [10.1093/mnras/stx2396](https://doi.org/10.1093/mnras/stx2396)
- Sneden, C. 1973, ApJ, 184, 839, doi: [10.1086/152374](https://doi.org/10.1086/152374)
- Sollima, A., Bellazzini, M., Smart, R. L., et al. 2009, MNRAS, 396, 2183, doi: [10.1111/j.1365-2966.2009.14864.x](https://doi.org/10.1111/j.1365-2966.2009.14864.x)
- Sollima, A., Ferraro, F. R., Pancino, E., & Bellazzini, M. 2005, MNRAS, 357, 265, doi: [10.1111/j.1365-2966.2005.08646.x](https://doi.org/10.1111/j.1365-2966.2005.08646.x)
- Starkenburg, E., Hill, V., Tolstoy, E., et al. 2010, A&A, 513, A34, doi: [10.1051/0004-6361/200913759](https://doi.org/10.1051/0004-6361/200913759)
- Suntzeff, N. B., & Kraft, R. P. 1996, AJ, 111, 1913, doi: [10.1086/117930](https://doi.org/10.1086/117930)
- Tolstoy, E., Hill, V., & Tosi, M. 2009, ARA&A, 47, 371, doi: [10.1146/annurev-astro-082708-101650](https://doi.org/10.1146/annurev-astro-082708-101650)
- van de Ven, G., van den Bosch, R. C. E., Verolme, E. K., & de Zeeuw, P. T. 2006, A&A, 445, 513, doi: [10.1051/0004-6361:20053061](https://doi.org/10.1051/0004-6361:20053061)
- van den Bergh, S. 1996, ApJL, 471, L31, doi: [10.1086/310331](https://doi.org/10.1086/310331)
- van Leeuwen, F., Le Poole, R. S., Reijns, R. A., Freeman, K. C., & de Zeeuw, P. T. 2000, A&A, 360, 472

- van Loon, J. T., van Leeuwen, F., Smalley, B., et al. 2007,  
MNRAS, 382, 1353,  
doi: [10.1111/j.1365-2966.2007.12478.x](https://doi.org/10.1111/j.1365-2966.2007.12478.x)
- Villanova, S., Geisler, D., Gratton, R. G., & Cassisi, S.  
2014, ApJ, 791, 107, doi: [10.1088/0004-637X/791/2/107](https://doi.org/10.1088/0004-637X/791/2/107)
- Villanova, S., Piotto, G., King, I. R., et al. 2007, ApJ, 663,  
296, doi: [10.1086/517905](https://doi.org/10.1086/517905)
- Wang, X., Jones, T. A., Treu, T., et al. 2019, ApJ, 882, 94,  
doi: [10.3847/1538-4357/ab3861](https://doi.org/10.3847/1538-4357/ab3861)
- Wolf, C., Onken, C. A., Luvaal, L. C., et al. 2018, PASA,  
35, e010, doi: [10.1017/pasa.2018.5](https://doi.org/10.1017/pasa.2018.5)
- Yong, D., Roederer, I. U., Grundahl, F., et al. 2014,  
MNRAS, 441, 3396, doi: [10.1093/mnras/stu806](https://doi.org/10.1093/mnras/stu806)

**Table 1.** Sky Coordinates, Photometry, Model Atmosphere Parameters, Iron Abundances, Errors, and Radial Velocities

LEID	RA	DEC	V	J	K <sub>S</sub>	T <sub>eff</sub>	log(g)	[Fe/H]	$\xi_{\text{mic.}}$	$\sigma/\sqrt{N}$	N	$\Delta[\text{Fe}/\text{H}]$	RV <sub>Helio.</sub>	Error
	(degrees)	(degrees)	(mag.)	(mag.)	(mag.)	(K)	(cgs)	(dex)	(km s <sup>-1</sup> )	(dex)		(dex)	(km s <sup>-1</sup> )	(km s <sup>-1</sup> )
4013	201.44247	-47.18851	13.982	12.111	11.511	4960	2.03	-1.49	1.46	0.05	14	0.12	220.6	0.4
4022	201.69444	-47.18516	14.635	12.745	12.158	4953	2.28	-1.43	1.46	0.03	14	0.12	220.1	0.6
6012	201.52474	-47.20504	13.685	11.881	11.278	5035	1.94	-1.95	1.41	0.05	12	0.14	232.2	0.3
7010	201.45608	-47.21242	14.662	12.858	12.307	5097	2.36	-1.72	1.37	0.03	12	0.14	236.9	0.7
7022	201.92768	-47.20907	14.338	12.399	11.790	4874	2.12	-1.85	1.51	0.06	12	0.14	205.1	0.4
8004	201.07113	-47.22082	14.508	12.687	12.007	4928	2.22	-1.48	1.48	0.02	13	0.12	244.3	0.3
8022	201.66668	-47.21645	14.034	12.085	11.454	4840	1.99	-1.74	1.53	0.05	13	0.14	244.9	0.3
8026	201.78482	-47.21673	14.315	12.397	11.785	4894	2.12	-1.77	1.50	0.04	13	0.14	229.3	0.5
8028	201.79297	-47.21472	13.931	12.172	11.652	5191	2.10	-1.44	1.31	0.06	10	0.13	222.4	0.9
9008	201.51840	-47.22127	13.851	12.241	11.747	5418	2.16	-1.79	1.16	0.05	11	0.14	237.8	0.4
10006	201.16314	-47.23357	13.710	11.887	11.300	5031	1.95	-1.90	1.41	0.05	12	0.14	239.8	0.3
10029	201.80897	-47.22988	14.296	12.359	11.726	4851	2.10	-1.79	1.53	0.04	13	0.14	225.4	0.3
11020	201.63017	-47.24044	13.851	11.896	11.230	4797	1.89	-1.52	1.56	0.03	13	0.14	229.9	0.4
12025	201.72957	-47.24688	14.224	12.406	11.781	4993	2.13	-1.64	1.43	0.05	11	0.14	235.4	1.1
13014	201.44182	-47.25608	14.195	12.239	11.598	4822	2.04	-1.48	1.55	0.03	12	0.12	226.2	0.7
13028	201.70258	-47.25524	14.434	12.627	12.030	5039	2.24	-1.67	1.41	0.03	11	0.14	218.7	0.3
14008	201.36780	-47.26070	13.650	11.911	11.370	5190	1.99	-1.33	1.31	0.04	12	0.12	252.9	0.4
14028	201.67091	-47.26057	13.706	11.755	11.122	4836	1.85	-1.75	1.54	0.05	12	0.14	226.5	0.3
14035	201.82702	-47.26180	14.142	12.243	11.618	4901	2.06	-1.46	1.49	0.03	12	0.12	221.6	0.9
14040	201.91045	-47.26064	13.869	12.079	11.527	5114	2.05	-1.70	1.36	0.04	10	0.14	239.5	0.3
14041	201.92318	-47.26065	14.307	12.388	11.745	4859	2.10	-1.61	1.52	0.05	13	0.14	237.0	0.3
14042	201.93956	-47.26221	14.475	12.588	11.947	...	...	...	...	...	...	...	232.4	2.0
15012	201.40686	-47.26967	14.251	12.411	11.778	4959	2.13	-1.70	1.46	0.04	13	0.14	225.4	0.4
15018	201.67301	-47.27263	13.782	11.987	11.402	5067	1.99	-1.74	1.39	0.04	13	0.14	209.1	0.3
17025	201.60253	-47.28719	13.809	12.073	11.509	5166	2.04	-1.90	1.32	0.05	10	0.14	253.4	0.4
18021	201.50836	-47.29494	13.530	11.682	11.063	4965	1.84	-1.84	1.45	0.03	12	0.14	242.1	0.3
18028	201.65542	-47.29263	13.768	11.830	11.176	4827	1.87	-1.72	1.54	0.03	13	0.14	228.5	0.3
18050	201.86680	-47.28925	14.232	12.626	12.125	5415	2.31	-1.90	1.16	0.07	8	0.15	223.9	0.4
19031	201.63658	-47.29775	13.915	12.058	11.443	4959	2.00	-1.54	1.46	0.03	12	0.14	237.3	0.3
19037	201.71141	-47.30118	14.420	12.583	11.975	4991	2.21	-1.78	1.44	0.03	13	0.14	235.3	0.4
19048	201.83571	-47.29851	14.183	12.325	11.719	4969	2.11	-1.52	1.45	0.04	13	0.14	230.5	0.3
19055	201.89532	-47.29739	13.592	11.794	11.163	5010	1.89	-1.58	1.42	0.05	12	0.14	239.1	0.4
19065	202.01444	-47.29983	14.539	12.641	12.004	4889	2.21	-1.43	1.50	0.04	13	0.12	243.0	0.5
20015	201.41369	-47.30916	14.284	12.494	11.904	5067	2.19	-1.66	1.39	0.05	12	0.14	255.6	0.7
20017	201.43875	-47.30781	14.064	12.253	11.610	4981	2.06	-1.70	1.44	0.04	12	0.14	234.6	0.4
20026	201.54652	-47.31119	14.351	12.533	11.924	5012	2.19	-1.65	1.42	0.03	12	0.14	227.8	0.3
20036	201.70374	-47.30357	14.117	12.275	11.640	4954	2.07	-1.70	1.46	0.04	13	0.14	230.2	0.3

**Table 1** *continued*

**Table 1** (*continued*)

LEID	RA	DEC	V	J	K <sub>S</sub>	T <sub>eff</sub>	log(g)	[Fe/H]	$\xi_{\text{mic.}}$	$\sigma/\sqrt{N}$	N	$\Delta[\text{Fe}/\text{H}]$	RV <sub>Helio.</sub>	Error
	(degrees)	(degrees)	(mag.)	(mag.)	(mag.)	(K)	(cgs)	(dex)	(km s <sup>-1</sup> )	(dex)		(dex)	(km s <sup>-1</sup> )	(km s <sup>-1</sup> )
21029	201.60882	-47.31443	14.046	12.452	11.925	5396	2.23	-1.73	1.17	0.05	11	0.14	234.5	0.4
21036	201.65793	-47.31665	14.488	12.690	12.073	5026	2.26	-1.57	1.41	0.04	12	0.14	224.8	0.3
22030	201.61720	-47.32318	14.479	12.695	12.094	5062	2.27	-1.65	1.39	0.04	12	0.14	245.5	0.5
22035	201.65267	-47.32575	14.410	12.570	11.933	4954	2.19	-1.67	1.46	0.03	11	0.14	220.5	0.3
22062	201.98775	-47.32039	14.320	12.426	11.815	4922	2.14	-1.79	1.48	0.05	10	0.14	215.9	0.3
23041	201.62290	-47.33342	14.121	12.400	11.688	5006	2.10	-1.56	1.43	0.04	12	0.14	239.6	0.3
23051	201.71487	-47.33170	14.355	12.466	11.839	4910	2.15	-1.79	1.49	0.02	13	0.13	238.7	0.4
23054	201.75562	-47.32885	13.815	12.124	11.555	5216	2.07	-1.74	1.29	0.05	10	0.14	233.8	0.3
23064	201.89567	-47.32890	14.096	12.129	11.493	4815	2.00	-1.72	1.55	0.05	11	0.14	246.3	0.6
24042	201.63385	-47.33654	13.553	11.651	10.971	4838	1.79	-1.82	1.53	0.02	13	0.13	239.3	0.3
24069	201.84379	-47.34082	13.695	11.905	11.315	5067	1.96	-1.55	1.39	0.03	13	0.14	234.8	0.8
25044	201.66382	-47.34868	14.442	12.608	11.974	4964	2.21	-1.75	1.45	0.04	11	0.14	230.5	0.3
26040	201.62653	-47.35031	13.907	12.079	11.460	4988	2.01	-1.56	1.44	0.02	13	0.13	229.5	0.4
26052	201.66562	-47.35633	14.165	12.359	11.723	4995	2.11	-1.74	1.43	0.03	12	0.14	231.1	0.3
26061	201.68779	-47.35565	14.425	12.562	11.959	4966	2.20	-1.75	1.45	0.03	13	0.14	249.7	0.3
27016	201.41071	-47.35936	14.622	12.848	12.267	5098	2.34	-1.57	1.37	0.05	12	0.14	232.8	0.4
27040	201.59212	-47.35953	13.797	11.861	11.199	4821	1.88	-1.70	1.55	0.04	13	0.14	233.1	0.3
27043	201.59750	-47.36325	14.092	12.284	11.664	5011	2.09	-1.54	1.42	0.06	13	0.14	231.7	0.5
27066	201.73032	-47.36012	14.394	12.874	12.389	5556	2.43	-1.82	1.07	0.06	7	0.15	211.1	0.5
27102	201.95822	-47.35650	14.269	12.628	12.153	...	...	...	...	...	...	...	229.5	0.6
28017	201.44673	-47.36660	14.277	12.445	11.862	5025	2.17	-1.58	1.41	0.04	12	0.14	233.8	0.4
28021	201.47546	-47.37077	14.417	12.581	11.951	4967	2.20	-1.73	1.45	0.04	13	0.14	232.5	0.3
28029	201.52547	-47.37133	14.095	12.194	11.549	4877	2.03	-1.52	1.51	0.04	13	0.14	236.7	0.4
28094	201.85231	-47.37121	13.837	11.910	11.276	4860	1.92	-1.75	1.52	0.04	12	0.14	249.2	0.9
28104	202.01604	-47.36317	13.866	11.886	11.212	4762	1.88	-1.61	1.58	0.04	12	0.14	229.4	0.6
29012	201.45369	-47.37645	13.692	11.734	11.068	4794	1.83	-1.81	1.56	0.02	12	0.13	230.3	0.3
29057	201.67804	-47.37545	14.060	12.260	11.610	4985	2.07	-1.80	1.44	0.04	12	0.14	246.0	0.3
29095	201.87980	-47.37223	14.302	12.461	11.798	4924	2.13	-1.75	1.48	0.04	12	0.14	240.2	0.7
29111	201.98572	-47.37736	14.323	12.426	11.776	4876	2.12	-1.70	1.51	0.05	11	0.14	224.8	0.9
30016	201.38634	-47.38739	14.285	12.421	11.790	4934	2.13	-1.50	1.47	0.04	13	0.14	235.9	0.4
30024	201.48549	-47.38079	14.139	12.299	11.720	5021	2.11	-1.57	1.42	0.04	12	0.14	222.2	0.4
30033	201.52477	-47.38331	14.216	12.414	11.798	5022	2.14	-1.53	1.42	0.05	11	0.14	232.2	0.4
30041	201.55331	-47.38549	13.973	12.123	11.506	4965	2.02	-1.71	1.45	0.03	12	0.14	224.3	0.3
30105	201.78461	-47.38307	14.145	12.304	11.703	4994	2.10	-1.69	1.43	0.04	12	0.14	209.7	0.4
31018	201.37651	-47.39283	13.631	11.702	11.079	4870	1.84	-1.67	1.51	0.04	13	0.14	217.0	1.1
31031	201.47083	-47.38866	13.887	11.949	11.311	4844	1.93	-1.68	1.53	0.04	11	0.14	240.9	0.4
31037	201.49467	-47.39425	13.806	11.844	11.198	4810	1.88	-1.60	1.55	0.02	13	0.13	230.1	0.4
31062	201.58966	-47.38771	14.423	12.568	11.953	4962	2.20	-1.21	1.45	0.04	12	0.12	217.9	0.6
31082	201.65619	-47.39125	13.507	11.608	10.951	4866	1.79	-1.70	1.52	0.04	13	0.14	255.1	0.3

**Table 1** *continued*

**Table 1** (*continued*)

LEID	RA	DEC	V	J	K <sub>S</sub>	T <sub>eff</sub>	log(g)	[Fe/H]	ξ <sub>mic.</sub>	σ/√N	N	Δ[Fe/H]	RV <sub>Helio.</sub>	Error
	(degrees)	(degrees)	(mag.)	(mag.)	(mag.)	(K)	(cgs)	(dex)	(km s <sup>-1</sup> )	(dex)		(dex)	(km s <sup>-1</sup> )	(km s <sup>-1</sup> )
31114	201.73152	-47.38935	13.756	12.089	11.542	5274	2.07	-1.76	1.25	0.04	10	0.14	221.1	1.8
32015	201.41028	-47.40040	12.411	10.896	10.393	5538	1.63	-1.98	1.08	0.04	9	0.14	226.9	1.1
32040	201.56659	-47.39700	14.161	12.381	11.746	5026	2.12	-1.71	1.41	0.04	11	0.14	244.1	0.4
32045	201.59365	-47.39851	14.361	12.549	11.918	4993	2.19	-1.43	1.43	0.03	13	0.12	230.8	0.4
33027	201.48522	-47.40622	13.824	12.133	11.567	5220	2.07	-1.87	1.29	0.04	11	0.14	208.0	0.5
33031	201.50705	-47.40851	14.437	12.578	11.921	4910	2.18	-1.37	1.49	0.03	12	0.12	225.1	0.4
33033	201.53108	-47.40287	14.228	12.418	11.817	5030	2.15	-1.69	1.41	0.03	10	0.14	227.1	0.3
33117	201.73694	-47.40605	13.321	11.536	10.928	5052	1.80	-1.92	1.40	0.07	9	0.15	232.2	0.4
33147	201.80917	-47.40322	13.837	11.863	11.216	4796	1.88	-1.87	1.56	0.04	13	0.14	235.9	0.5
34012	201.31212	-47.41251	14.370	12.560	11.942	5011	2.20	-1.51	1.42	0.04	13	0.14	222.7	0.4
34015	201.40628	-47.41161	14.457	12.570	11.937	4906	2.19	-1.85	1.49	0.03	12	0.14	235.0	0.7
34018	201.42983	-47.41121	14.319	12.425	11.822	4931	2.14	-1.75	1.47	0.04	11	0.14	240.9	0.3
34033	201.52815	-47.41256	14.207	12.385	11.820	5059	2.16	-1.64	1.39	0.03	9	0.14	215.4	0.4
34063	201.59383	-47.41040	13.711	11.850	11.194	4909	1.89	-1.68	1.49	0.04	13	0.14	221.2	0.6
34202	201.83066	-47.41326	14.141	12.550	12.023	5400	2.27	-1.78	1.17	0.04	10	0.14	229.9	0.3
35038	201.45658	-47.41751	13.693	11.711	11.064	4788	1.82	-1.86	1.57	0.04	11	0.14	242.5	0.5
35051	201.51153	-47.41889	13.698	11.804	11.172	4899	1.88	-1.62	1.50	0.03	13	0.14	214.7	0.3
35076	201.57772	-47.41723	14.010	12.188	11.561	4986	2.05	-1.52	1.44	0.05	13	0.14	211.4	0.4
35206	201.75761	-47.41718	14.195	12.367	11.713	4949	2.10	-1.86	1.46	0.04	12	0.14	247.7	1.1
35268	202.03099	-47.42299	14.167	12.196	11.549	4800	2.02	-1.72	1.56	0.04	11	0.14	232.7	0.6
36020	201.43352	-47.42713	14.425	12.573	11.955	4962	2.20	-1.56	1.45	0.03	13	0.14	236.9	0.3
36024	201.48592	-47.42517	14.191	12.330	11.750	4995	2.12	-1.39	1.43	0.03	13	0.12	225.9	0.4
36032	201.53233	-47.43151	14.203	12.357	11.762	4995	2.13	-1.56	1.43	0.05	11	0.14	254.9	0.5
36037	201.54602	-47.43044	14.122	12.099	11.567	4865	2.03	-1.81	1.52	0.04	12	0.14	244.5	0.4
36043	201.57655	-47.42716	13.944	12.132	11.544	5043	2.05	-1.53	1.40	0.05	12	0.14	214.1	0.3
36051	201.59115	-47.42981	14.467	12.618	12.055	5029	2.25	-1.52	1.41	0.04	9	0.14	238.8	0.8
36058	201.60027	-47.42722	13.829	11.978	11.325	4924	1.94	-1.71	1.48	0.04	12	0.14	222.5	0.5
36095	201.64704	-47.42934	13.298	11.390	10.704	4826	1.68	-1.74	1.54	0.03	13	0.14	219.7	0.3
36097	201.64935	-47.42799	14.031	12.252	11.644	5059	2.09	-1.93	1.39	0.05	9	0.14	221.2	0.9
36159	201.71318	-47.42592	14.244	12.508	11.920	5137	2.21	-1.47	1.34	0.03	12	0.12	213.2	1.1
36175	201.72638	-47.42917	14.265	12.438	11.777	4942	2.13	-1.81	1.47	0.05	11	0.14	235.5	0.6
36203	201.76517	-47.42612	14.014	12.214	11.576	...	...	...	...	...	...	...	219.8	0.7
36243	201.83821	-47.42440	14.251	12.345	11.694	4865	2.08	-1.49	1.52	0.02	13	0.12	242.5	0.4
36255	201.85339	-47.42474	14.251	12.384	11.766	4945	2.12	-1.75	1.47	0.04	12	0.14	223.6	0.6
36258	201.85705	-47.42666	14.315	12.397	11.743	4849	2.10	-1.79	1.53	0.02	12	0.13	239.4	0.5
36276	201.90026	-47.42541	14.137	12.284	11.658	4952	2.08	-1.80	1.46	0.04	12	0.14	236.4	0.4
36278	201.91641	-47.42488	13.820	12.067	11.505	5148	2.04	-1.80	1.33	0.04	10	0.14	247.7	1.1
37023	201.44027	-47.43511	14.443	12.615	12.061	5064	2.25	-1.50	1.39	0.02	10	0.13	219.5	0.5
37027	201.45894	-47.43578	14.228	12.403	11.812	5024	2.15	-1.71	1.41	0.03	12	0.14	229.8	0.3

**Table 1** *continued*

**Table 1** (*continued*)

LEID	RA	DEC	V	J	K <sub>S</sub>	T <sub>eff</sub>	log(g)	[Fe/H]	$\xi_{\text{mic.}}$	$\sigma/\sqrt{N}$	N	$\Delta[\text{Fe}/\text{H}]$	RV <sub>Helio.</sub>	Error
	(degrees)	(degrees)	(mag.)	(mag.)	(mag.)	(K)	(cgs)	(dex)	(km s <sup>-1</sup> )	(dex)	(dex)	(km s <sup>-1</sup> )	(km s <sup>-1</sup> )	
37038	201.50406	-47.43944	14.456	12.580	11.948	4919	2.19	-1.54	1.48	0.04	13	0.14	236.7	0.4
37043	201.53100	-47.43611	14.380	12.570	11.959	5019	2.21	-1.71	1.42	0.04	10	0.14	239.4	0.3
37044	201.53863	-47.43623	14.230	12.450	11.867	5088	2.18	-1.60	1.37	0.05	10	0.14	217.7	0.4
37048	201.55376	-47.43404	14.186	12.377	11.779	5035	2.14	-1.54	1.41	0.04	10	0.14	233.1	0.3
37059	201.58576	-47.43315	13.930	12.111	11.461	4964	2.00	-1.60	1.45	0.04	13	0.14	238.8	0.3
37072	201.60695	-47.43960	14.347	12.824	12.320	5525	2.40	-2.03	1.09	0.09	4	0.16	248.4	0.5
37099	201.63168	-47.43614	14.002	12.555	11.888	5408	2.22	-1.46	1.17	0.05	9	0.12	220.4	0.7
37104	201.63899	-47.43193	14.192	12.342	11.762	...	...	...	...	...	...	...	231.2	1.1
37183	201.70897	-47.43702	13.717	11.755	11.113	4814	1.85	-1.70	1.55	0.05	12	0.14	211.2	0.3
37223	201.73871	-47.43699	14.312	12.511	11.874	4999	2.17	-1.86	1.43	0.05	12	0.14	231.0	0.4
37262	201.77927	-47.43276	14.174	12.497	11.933	5240	2.22	-1.61	1.27	0.04	12	0.14	255.0	0.4
37287	201.81556	-47.43386	12.883	10.783	10.060	4597	1.40	-1.80	1.69	0.03	13	0.14	226.6	0.3
38032	201.51473	-47.44189	13.815	12.214	11.710	5417	2.15	-1.75	1.16	0.04	10	0.14	229.9	1.2
38036	201.53299	-47.44377	14.389	12.575	11.990	5044	2.22	-1.67	1.40	0.04	10	0.14	247.8	0.3
38135	201.66470	-47.44132	13.315	11.575	10.958	5096	1.82	-1.75	1.37	0.04	12	0.14	232.6	0.3
38155	201.68262	-47.44376	14.293	99.999	99.999	4905	2.12	-1.91	1.49	0.04	11	0.14	229.6	0.4
38164	201.68948	-47.43944	13.845	11.615	11.400	4984	1.98	-1.61	1.44	0.03	10	0.14	238.9	0.6
38307	201.79761	-47.44688	14.387	13.005	12.488	5711	2.48	-0.81	0.97	0.05	13	0.11	249.3	0.5
38309	201.79846	-47.44037	14.131	12.313	11.713	5022	2.11	-0.97	1.42	0.08	8	0.13	237.5	0.4
38318	201.81336	-47.44301	13.516	11.634	11.010	4921	1.82	-1.97	1.48	0.05	11	0.14	255.9	0.6
38352	201.97004	-47.44269	13.512	11.615	11.010	...	...	...	...	...	...	...	246.5	0.3
38358	202.02845	-47.43972	14.382	12.865	12.387	5570	2.43	-2.14	1.06	0.06	7	0.15	238.8	0.6
39020	201.29048	-47.45508	13.741	11.835	11.197	4879	1.89	-1.77	1.51	0.03	11	0.14	230.0	0.3
39030	201.39691	-47.44988	14.191	12.469	11.890	5165	2.20	-2.01	1.32	0.05	11	0.14	233.1	0.4
39046	201.51347	-47.45357	13.042	11.261	10.687	5098	1.71	-1.74	1.37	0.03	10	0.14	253.0	0.3
39054	201.53397	-47.44775	14.487	13.072	12.662	5822	2.56	-1.57	0.90	0.04	10	0.14	222.3	0.2
39114	201.61253	-47.45104	14.299	12.839	12.352	...	...	...	...	...	...	...	233.8	0.9
39159	201.64595	-47.45127	13.594	11.770	11.205	5056	1.91	-1.58	1.39	0.03	10	0.14	230.1	1.0
39160	201.64740	-47.44837	14.148	12.401	11.755	5053	2.13	-1.42	1.40	0.04	12	0.12	252.8	0.8
39183	201.66459	-47.45215	13.490	11.689	11.051	4998	1.84	-1.96	1.43	0.05	9	0.14	230.8	0.6
39219	201.68658	-47.44704	12.985	10.981	10.302	4733	1.51	-1.60	1.60	0.04	13	0.14	233.3	1.9
39234	201.69320	-47.45213	12.910	10.791	10.040	4561	1.39	-2.00	1.71	0.02	11	0.13	245.0	0.4
39281	201.71736	-47.45365	13.681	11.950	11.383	5169	1.99	-1.51	1.32	0.05	12	0.14	234.8	0.3
39309	201.73811	-47.45247	13.661	11.643	11.015	4770	1.80	-2.50	1.58	0.05	11	0.14	242.4	0.4
39363	201.78667	-47.45088	13.769	11.928	11.282	4943	1.93	-1.78	1.47	0.04	10	0.14	203.4	0.3
39406	201.85778	-47.44707	13.695	11.892	11.311	5062	1.95	-1.87	1.39	0.04	10	0.14	240.2	0.7
40008	201.28278	-47.45599	14.189	12.180	11.523	4750	2.00	-1.50	1.59	0.02	13	0.13	251.1	0.3
40028	201.45841	-47.46064	13.962	12.090	11.447	4911	1.99	-1.91	1.49	0.04	10	0.14	224.9	0.3
40030	201.46704	-47.45655	14.663	12.869	12.343	5141	2.38	-1.62	1.34	0.04	13	0.14	229.4	0.6

**Table 1** *continued*

**Table 1** (*continued*)

LEID	RA	DEC	V	J	K <sub>S</sub>	T <sub>eff</sub>	log(g)	[Fe/H]	$\xi_{\text{mic.}}$	$\sigma/\sqrt{N}$	N	$\Delta[\text{Fe}/\text{H}]$	RV <sub>Helio.</sub>	Error
	(degrees)	(degrees)	(mag.)	(mag.)	(mag.)	(K)	(cgs)	(dex)	(km s <sup>-1</sup> )	(dex)	(dex)	(km s <sup>-1</sup> )	(km s <sup>-1</sup> )	
40045	201.53151	-47.45737	13.475	11.569	10.944	4893	1.79	-1.68	1.50	0.04	13	0.14	224.4	0.3
40047	201.53223	-47.46138	13.569	11.650	11.020	4873	1.82	-1.53	1.51	0.04	12	0.14	220.2	0.3
40055	201.55656	-47.45951	14.157	12.342	11.715	4994	2.11	-1.74	1.43	0.05	10	0.14	201.6	0.4
40069	201.57362	-47.46253	14.392	13.083	12.702	...	...	...	...	...	...	...	259.4	0.8
40129	201.63316	-47.45951	14.074	12.256	11.578	4933	2.05	-1.77	1.47	0.02	11	0.13	223.0	0.5
40175	201.65817	-47.45646	13.381	11.273	10.329	4414	1.49	-2.50	1.81	0.05	11	0.14	221.6	0.8
40180	201.66068	-47.45642	14.375	12.472	11.775	...	...	...	...	...	...	...	220.8	1.9
40219	201.67663	-47.46117	13.177	11.329	10.687	4939	1.69	-1.74	1.47	0.04	11	0.14	218.3	0.5
40249	201.69299	-47.45999	14.051	12.237	11.588	4970	2.05	-1.86	1.45	0.03	11	0.14	248.8	0.4
40279	201.70587	-47.45789	13.097	11.023	10.308	4629	1.50	-1.85	1.67	0.01	12	0.13	210.1	0.3
40295	201.71174	-47.45937	13.304	11.339	10.661	4774	1.66	-2.16	1.58	0.03	11	0.14	206.8	0.4
40300	201.71378	-47.45719	14.230	12.365	11.822	...	...	...	...	...	...	...	209.2	0.6
40301	201.71392	-47.45495	13.831	11.885	11.169	4755	1.86	-2.08	1.59	0.04	12	0.14	225.9	0.4
40311	201.71853	-47.45987	13.552	11.746	11.098	4981	1.86	-1.95	1.44	0.04	12	0.14	242.5	0.4
40463	201.88460	-47.45819	14.176	12.455	11.919	5219	2.21	-2.04	1.29	0.05	10	0.14	237.3	0.5
40481	201.96171	-47.45389	13.900	12.191	11.668	5251	2.12	-1.98	1.27	0.02	8	0.13	235.9	0.5
41037	201.45566	-47.46877	14.450	12.660	12.048	5041	2.25	-1.70	1.40	0.03	11	0.14	227.7	0.7
41056	201.52534	-47.46639	14.449	12.630	12.029	5020	2.24	-1.39	1.42	0.03	10	0.12	229.0	0.4
41068	201.55448	-47.46479	14.217	12.525	11.988	5255	2.25	-1.16	1.27	0.06	9	0.13	198.0	1.0
41100	201.60006	-47.46929	13.523	11.681	11.042	4950	1.83	-1.80	1.46	0.02	11	0.13	218.0	0.3
41139	201.62823	-47.46595	13.337	11.286	10.598	4677	1.63	-1.82	1.64	0.03	11	0.14	253.0	1.2
41140	201.62859	-47.46718	12.321	10.134	9.355	4480	1.10	-1.96	1.77	0.02	12	0.13	226.0	0.3
41157	201.64021	-47.46664	14.045	12.698	12.022	5534	2.28	-0.88	1.08	0.05	10	0.11	226.4	0.5
41162	201.64342	-47.46544	14.067	99.999	99.999	...	...	...	...	...	...	...	197.5	1.3
41171	201.64731	-47.46420	13.867	11.964	11.302	4857	1.93	-1.34	1.52	0.02	13	0.12	212.5	0.4
41179	201.65113	-47.46830	13.811	12.009	11.121	4729	1.84	-2.35	1.61	0.04	11	0.14	208.6	0.3
41205	201.66382	-47.46953	14.134	12.315	11.691	4993	2.10	-1.57	1.43	0.04	11	0.14	236.6	0.6
41224	201.67256	-47.46648	13.247	11.156	10.410	4584	1.54	-1.90	1.70	0.03	10	0.13	212.4	0.6
41234	201.67791	-47.46711	13.635	11.879	11.239	5049	1.92	-1.54	1.40	0.03	9	0.14	230.9	0.4
41265	201.69279	-47.46851	13.339	11.240	10.437	4534	1.54	-2.41	1.73	0.03	10	0.14	257.8	0.4
41301	201.71083	-47.46861	13.259	11.262	10.582	4739	1.62	-1.70	1.60	0.04	12	0.14	271.1	0.6
41317	201.71686	-47.46540	13.860	11.897	11.179	4735	1.86	-2.10	1.60	0.05	10	0.14	234.7	0.5
41323	201.71949	-47.46918	13.375	11.379	10.617	4659	1.63	-2.14	1.65	0.04	12	0.14	228.5	0.3
41328	201.72165	-47.46376	14.272	12.736	12.127	...	...	...	...	...	...	...	228.8	0.8
41331	201.72388	-47.46735	13.499	11.644	11.022	4954	1.83	-1.92	1.46	0.05	11	0.14	250.5	0.3
41338	201.72804	-47.46432	14.081	12.262	11.610	4961	2.06	-1.85	1.46	0.02	11	0.13	235.9	0.3
41374	201.74611	-47.46323	13.428	11.515	10.829	4820	1.73	-1.77	1.55	0.04	11	0.14	250.8	0.3
41427	201.78341	-47.46329	14.133	12.744	12.288	...	...	...	...	...	...	...	253.6	0.6
41437	201.79138	-47.46561	14.500	12.757	12.314	5309	2.38	-1.51	1.23	0.05	8	0.14	239.3	0.6

**Table 1** *continued*

**Table 1** (*continued*)

LEID	RA	DEC	V	J	K <sub>S</sub>	T <sub>eff</sub>	log(g)	[Fe/H]	$\xi_{\text{mic.}}$	$\sigma/\sqrt{N}$	N	$\Delta[\text{Fe}/\text{H}]$	RV <sub>Helio.</sub>	Error
	(degrees)	(degrees)	(mag.)	(mag.)	(mag.)	(K)	(cgs)	(dex)	(km s <sup>-1</sup> )	(dex)	(dex)	(km s <sup>-1</sup> )	(km s <sup>-1</sup> )	
41478	201.85750	-47.46839	14.123	12.568	12.038	5445	2.28	-1.66	1.14	0.05	9	0.14	228.4	0.4
41509	202.02779	-47.46745	14.174	12.239	11.632	4881	2.06	-1.79	1.51	0.03	10	0.14	251.9	0.4
42025	201.46468	-47.47735	13.679	11.736	11.095	4836	1.84	-1.81	1.54	0.03	12	0.14	230.0	0.3
42032	201.49242	-47.47554	14.183	12.301	11.709	4957	2.10	-1.74	1.46	0.03	10	0.14	237.0	0.3
42065	201.56859	-47.47507	14.238	12.652	12.066	5330	2.28	-1.44	1.22	0.03	8	0.12	214.2	0.9
42119	201.62091	-47.47195	14.064	12.148	11.522	4881	2.02	-1.59	1.51	0.04	11	0.14	222.6	0.6
42124	201.62389	-47.47390	13.407	11.603	10.936	...	...	...	...	...	...	...	203.0	0.6
42131	201.62780	-47.47064	13.973	11.368	10.695	4910	2.00	-1.70	1.49	0.06	7	0.15	196.3	0.9
42158	201.64343	-47.47615	14.246	12.151	11.474	4645	1.97	-1.54	1.66	0.05	9	0.14	225.0	0.6
42171	201.65129	-47.47293	13.742	11.818	11.148	4825	1.86	-1.96	1.54	0.04	10	0.14	241.2	0.5
42178	201.65447	-47.47389	14.368	99.999	99.999	4926	2.16	-1.79	1.48	0.06	10	0.15	215.2	0.9
42184	201.65710	-47.47548	13.952	99.999	99.999	4915	1.99	-1.78	1.49	0.05	11	0.14	241.5	0.2
42193	201.66296	-47.47630	14.487	13.123	12.773	...	...	...	...	...	...	...	222.7	0.6
42203	201.66732	-47.47358	14.016	12.316	11.691	5136	2.12	-1.67	1.34	0.04	11	0.14	192.9	0.6
42223	201.67616	-47.47493	13.871	12.167	11.622	5229	2.10	-1.74	1.28	0.05	10	0.14	248.5	0.3
42245	201.68489	-47.47360	13.655	11.852	11.261	5051	1.93	-1.73	1.40	0.05	8	0.14	199.6	0.8
42268	201.69523	-47.47334	14.126	12.312	11.670	4978	2.09	-2.21	1.44	0.06	10	0.15	246.4	1.9
42272	201.69778	-47.47186	13.831	11.925	10.585	4925	1.95	-1.79	1.48	0.04	9	0.14	222.8	1.0
42314	201.71214	-47.47268	14.308	12.532	11.923	5062	2.20	-1.74	1.39	0.04	10	0.14	229.0	0.4
42317	201.71346	-47.47610	13.624	11.310	10.588	4424	1.60	-2.21	1.80	0.03	10	0.14	233.6	0.4
42333	201.72101	-47.47531	13.401	11.307	10.605	4622	1.62	-2.37	1.67	0.03	10	0.14	241.8	0.4
42355	201.73550	-47.47057	13.752	11.566	10.958	4622	1.76	-2.38	1.67	0.03	12	0.14	223.5	0.4
42387	201.75225	-47.47556	13.372	10.707	9.755	...	...	...	...	...	...	...	231.5	0.3
42401	201.76274	-47.47304	13.048	11.525	10.925	5395	1.83	-1.63	1.17	0.05	10	0.14	256.0	0.4
42420	201.77644	-47.47119	14.387	12.400	11.796	4828	2.12	-1.87	1.54	0.03	11	0.14	246.0	1.2
42502	201.89481	-47.47509	14.495	12.540	11.950	4877	2.19	-1.85	1.51	0.05	11	0.14	207.6	0.8
42510	201.95694	-47.47643	13.837	11.913	11.294	4880	1.93	-1.55	1.51	0.03	12	0.14	232.3	0.4
43025	201.45411	-47.47994	14.246	12.387	11.797	4986	2.14	-1.70	1.44	0.04	12	0.14	241.5	0.4
43038	201.50916	-47.48003	13.663	11.754	11.107	4866	1.85	-1.86	1.52	0.03	11	0.14	243.8	1.0
43057	201.53786	-47.48474	14.344	12.502	11.939	5037	2.20	-1.54	1.41	0.07	8	0.15	232.1	1.5
43103	201.60935	-47.47884	14.267	12.532	11.928	...	...	...	...	...	...	...	218.6	1.8
43105	201.61359	-47.47978	11.935	10.689	10.063	...	...	...	...	...	...	...	228.2	0.5
43107	201.61477	-47.48463	14.045	12.322	11.731	...	...	...	...	...	...	...	206.8	1.6
43136	201.63454	-47.48062	13.797	12.001	11.419	...	...	...	...	...	...	...	222.0	1.2
43153	201.64700	-47.48038	14.177	12.322	11.767	...	...	...	...	...	...	...	243.4	0.6
43167	201.65370	-47.48043	14.448	12.632	12.017	5007	2.23	-1.73	1.43	0.07	6	0.15	261.2	0.7
43212	201.67336	-47.47986	13.393	11.722	11.124	5205	1.90	-2.11	1.30	0.06	9	0.14	227.8	0.5
43227	201.67864	-47.48253	13.439	11.569	10.846	4827	1.74	-1.68	1.54	0.06	9	0.15	236.7	0.7
43244	201.68551	-47.48218	13.362	11.275	10.570	4626	1.61	-2.14	1.67	0.07	8	0.15	251.9	0.8

**Table 1** *continued*

**Table 1** (*continued*)

LEID	RA	DEC	V	J	K <sub>S</sub>	T <sub>eff</sub>	log(g)	[Fe/H]	$\xi_{\text{mic.}}$	$\sigma/\sqrt{N}$	N	$\Delta[\text{Fe}/\text{H}]$	RV <sub>Helio.</sub>	Error
	(degrees)	(degrees)	(mag.)	(mag.)	(mag.)	(K)	(cgs)	(dex)	(km s <sup>-1</sup> )	(dex)		(dex)	(km s <sup>-1</sup> )	(km s <sup>-1</sup> )
43271	201.69447	-47.48023	13.375	11.465	10.837	4886	1.74	-1.64	1.50	0.04	10	0.14	209.7	0.7
43303	201.70747	-47.48416	13.785	11.830	11.239	4876	1.90	-1.70	1.51	0.03	12	0.14	186.7	0.4
43338	201.72265	-47.47787	13.463	11.593	10.861	4818	1.75	-1.49	1.55	0.02	13	0.12	244.7	0.4
43344	201.72576	-47.48195	13.710	12.007	11.404	5159	2.00	-1.80	1.33	0.04	11	0.14	232.1	0.4
43380	201.74145	-47.48222	13.224	11.215	10.248	4474	1.46	-2.36	1.77	0.03	12	0.14	257.4	0.6
43402	201.75295	-47.48133	13.616	11.767	11.492	5387	2.06	-1.50	1.18	0.04	10	0.14	245.4	0.5
43415	201.76232	-47.48037	13.703	11.935	11.313	5056	1.95	-1.86	1.39	0.05	10	0.14	269.7	0.3
43430	201.77079	-47.48290	14.305	11.547	12.009	5153	2.24	-2.03	1.33	0.04	13	0.14	245.0	0.4
43445	201.77809	-47.48069	14.426	99.999	99.999	...	...	...	...	...	...	...	227.5	0.4
44013	201.28650	-47.48931	14.326	12.436	11.791	4889	2.13	-1.91	1.50	0.03	10	0.14	228.7	0.4
44016	201.35303	-47.48591	14.393	12.517	11.895	4930	2.17	-1.77	1.48	0.03	13	0.14	220.0	0.3
44021	201.38691	-47.48594	13.927	11.981	11.374	4869	1.96	-1.83	1.51	0.03	13	0.14	220.8	0.3
44028	201.46219	-47.48922	14.471	12.601	12.022	4985	2.23	-1.43	1.44	0.04	13	0.12	235.5	0.4
44073	201.57501	-47.48562	14.061	12.240	11.620	4995	2.07	-1.64	1.43	0.06	11	0.14	229.7	1.4
44091	201.59398	-47.49202	14.255	12.505	11.843	...	...	...	...	...	...	...	242.4	1.0
44144	201.63273	-47.49183	13.527	11.627	10.933	4826	1.78	-1.80	1.54	0.04	13	0.14	231.9	0.3
44154	201.64379	-47.48883	14.038	12.101	10.721	...	...	...	...	...	...	...	224.3	0.4
44156	201.64606	-47.49021	13.273	11.403	10.757	4910	1.72	-1.92	1.49	0.06	9	0.14	249.9	0.4
44164	201.64891	-47.48773	14.348	11.640	11.961	5043	2.21	-1.72	1.40	0.04	9	0.14	223.6	0.6
44182	201.65777	-47.48604	14.060	12.240	11.565	...	...	...	...	...	...	...	227.7	1.9
44186	201.66003	-47.48737	14.341	12.518	11.888	4982	2.18	-1.81	1.44	0.04	6	0.14	219.2	0.7
44232	201.67861	-47.49017	13.394	11.499	10.867	4898	1.76	-2.01	1.50	0.06	9	0.15	232.6	0.5
44238	201.68099	-47.48556	13.790	12.504	11.935	...	...	...	...	...	...	...	239.2	0.8
44241	201.68201	-47.49233	13.245	11.273	10.646	4819	1.66	-2.03	1.55	0.05	11	0.14	237.6	0.5
44252	201.68863	-47.49011	13.150	11.058	10.349	...	...	...	...	...	...	...	228.6	1.2
44299	201.70771	-47.48586	13.165	11.221	10.553	4806	1.62	-1.84	1.56	0.04	12	0.14	253.6	0.3
44324	201.71748	-47.49016	13.893	12.260	11.677	5272	2.12	-2.01	1.25	0.05	8	0.14	256.4	0.6
44336	201.72279	-47.48893	13.378	11.360	10.664	4702	1.65	-1.90	1.62	0.03	12	0.14	221.2	0.8
44348	201.72762	-47.48853	14.286	12.304	11.711	...	...	...	...	...	...	...	228.0	0.8
44409	201.76483	-47.48878	14.323	12.170	11.583	4674	2.02	-2.17	1.64	0.05	11	0.14	236.0	0.4
44513	201.98859	-47.48558	13.428	11.492	10.835	4826	1.74	-1.84	1.54	0.02	10	0.13	240.5	0.3
45017	201.27556	-47.49757	14.370	12.582	11.980	5056	2.22	-1.89	1.39	0.03	11	0.14	230.9	0.3
45018	201.28748	-47.49684	13.775	12.039	11.440	5124	2.01	-1.75	1.35	0.04	11	0.14	234.5	0.3
45034	201.47309	-47.49553	14.142	12.246	11.628	4912	2.06	-1.73	1.49	0.03	10	0.14	226.2	0.4
45054	201.55044	-47.49329	13.556	11.665	11.013	4880	1.81	-1.63	1.51	0.04	12	0.14	218.6	0.3
45146	201.63892	-47.49504	14.040	12.085	11.348	...	...	...	...	...	...	...	222.5	1.3
45147	201.63892	-47.49632	13.721	99.999	99.999	...	...	...	...	...	...	...	223.2	6.1
45167	201.65004	-47.49888	14.390	12.338	11.713	...	...	...	...	...	...	...	224.8	1.0
45169	201.65041	-47.49585	13.501	11.538	10.878	4795	1.75	-1.85	1.56	0.03	13	0.14	232.8	0.3

**Table 1** *continued*

**Table 1** (*continued*)

LEID	RA	DEC	V	J	K <sub>S</sub>	T <sub>eff</sub>	log(g)	[Fe/H]	$\xi_{\text{mic.}}$	$\sigma/\sqrt{N}$	N	$\Delta[\text{Fe}/\text{H}]$	RV <sub>Helio.</sub>	Error
	(degrees)	(degrees)	(mag.)	(mag.)	(mag.)	(K)	(cgs)	(dex)	(km s <sup>-1</sup> )	(dex)	(dex)	(km s <sup>-1</sup> )	(km s <sup>-1</sup> )	
45186	201.66127	-47.49911	14.165	12.252	11.580	4835	2.04	-1.75	1.54	0.05	10	0.14	248.6	1.2
45214	201.67405	-47.49979	14.319	12.548	11.880	4999	2.18	-1.66	1.43	0.05	11	0.14	228.0	0.4
45216	201.67534	-47.49401	13.510	99.999	99.999	...	...	...	...	...	...	...	237.2	1.2
45241	201.68610	-47.49857	13.442	11.489	10.888	4868	1.76	-1.79	1.52	0.06	11	0.15	229.0	0.8
45251	201.69122	-47.49916	14.276	99.999	99.999	...	...	...	...	...	...	...	217.4	5.5
45261	201.69548	-47.49276	13.397	11.274	10.611	4631	1.62	-2.18	1.67	0.04	11	0.14	215.5	0.3
45284	201.70556	-47.49660	13.704	11.782	11.049	4762	1.81	-1.11	1.58	0.03	13	0.12	211.6	0.5
45301	201.71431	-47.49728	13.481	11.419	10.837	4771	1.73	-2.24	1.58	0.05	12	0.14	219.0	0.4
45302	201.71548	-47.49633	14.077	12.381	11.816	5215	2.17	-1.59	1.29	0.04	12	0.14	241.5	0.6
45314	201.71936	-47.49717	14.005	12.101	11.402	4816	1.96	-1.95	1.55	0.03	12	0.14	259.3	0.3
45347	201.73373	-47.49359	14.400	12.080	11.466	...	...	...	...	...	...	...	235.2	0.6
45352	201.73629	-47.49777	13.213	11.192	10.489	4692	1.58	-1.67	1.63	0.03	13	0.14	251.4	0.4
45368	201.74348	-47.49684	14.337	12.662	11.965	...	...	...	...	...	...	...	244.8	5.1
45405	201.76391	-47.49236	13.863	12.039	11.432	5007	2.00	-1.65	1.43	0.03	10	0.13	247.1	0.4
45456	201.80205	-47.49403	14.070	12.125	11.498	4848	2.00	-1.79	1.53	0.03	11	0.14	242.6	0.3
45486	201.84500	-47.49383	14.455	12.630	12.019	5001	2.23	-1.64	1.43	0.05	11	0.14	251.6	0.4
45516	201.98842	-47.49232	14.363	12.474	11.846	4909	2.15	-1.18	1.49	0.04	12	0.12	236.9	0.8
46132	201.63590	-47.50027	13.673	11.751	11.050	4795	1.82	-1.67	1.56	0.03	12	0.14	219.4	0.4
46135	201.63877	-47.50480	13.388	11.417	10.746	4775	1.69	-1.40	1.58	0.04	12	0.12	207.5	0.4
46157	201.65318	-47.50621	13.087	11.004	10.274	4606	1.49	-1.86	1.68	0.03	13	0.14	204.0	0.5
46177	201.66534	-47.50542	13.424	11.481	10.809	4803	1.72	-1.88	1.56	0.04	9	0.14	232.4	0.9
46188	201.66944	-47.50143	14.320	12.462	11.898	5017	2.18	-2.30	1.42	0.05	10	0.14	214.1	1.0
46224	201.68777	-47.50313	13.367	11.289	9.575	...	...	...	...	...	...	...	240.7	0.8
46226	201.68893	-47.50708	13.258	11.194	10.528	4685	1.59	-1.65	1.63	0.04	11	0.14	245.9	0.5
46228	201.68907	-47.50077	14.396	12.247	11.637	...	...	...	...	...	...	...	236.0	1.3
46239	201.69750	-47.50687	13.652	11.717	11.041	4807	1.82	-1.85	1.55	0.06	11	0.14	233.3	0.4
46252	201.70584	-47.50640	13.546	11.872	11.316	...	...	...	...	...	...	...	245.5	0.5
46257	201.70725	-47.50674	14.141	11.657	10.911	4282	1.71	-1.52	1.89	0.05	10	0.14	233.0	0.6
46299	201.72807	-47.50100	14.088	12.406	11.829	...	...	...	...	...	...	...	232.5	0.4
46310	201.73488	-47.50350	13.563	11.706	11.122	4995	1.87	-1.87	1.43	0.06	10	0.15	226.4	0.4
46330	201.74252	-47.50373	13.746	11.207	11.148	4812	1.86	-2.52	1.55	0.03	11	0.14	225.5	0.4
46332	201.74307	-47.50299	14.179	11.365	11.708	4945	2.09	-1.68	1.47	0.04	10	0.14	243.6	0.4
46344	201.75154	-47.50503	13.547	11.593	10.811	4681	1.71	-1.97	1.64	0.03	11	0.14	211.7	0.3
46357	201.75898	-47.50317	13.247	11.189	10.483	4653	1.58	-1.86	1.65	0.03	12	0.14	236.1	0.4
46360	201.76205	-47.50125	13.500	11.515	10.859	4776	1.74	-1.89	1.57	0.03	12	0.14	262.2	0.5
47027	201.47443	-47.51170	14.383	12.514	11.902	4949	2.18	-1.75	1.46	0.03	11	0.14	227.2	0.3
47093	201.60651	-47.50779	13.362	11.385	10.681	4735	1.66	-1.86	1.60	0.02	12	0.13	214.4	0.4
47214	201.68680	-47.51002	14.280	12.432	11.856	5015	2.17	-1.65	1.42	0.05	10	0.14	222.3	0.5
47221	201.69115	-47.51349	13.931	12.081	11.499	5005	2.02	-1.76	1.43	0.04	9	0.14	222.4	0.5

**Table 1** *continued*

**Table 1** (*continued*)

LEID	RA	DEC	V	J	K <sub>S</sub>	T <sub>eff</sub>	log(g)	[Fe/H]	$\xi_{\text{mic.}}$	$\sigma/\sqrt{N}$	N	$\Delta[\text{Fe}/\text{H}]$	RV <sub>Helio.</sub>	Error
	(degrees)	(degrees)	(mag.)	(mag.)	(mag.)	(K)	(cgs)	(dex)	(km s <sup>-1</sup> )	(dex)	(dex)	(km s <sup>-1</sup> )	(km s <sup>-1</sup> )	
47241	201.69938	-47.50952	14.333	12.637	11.989	5114	2.23	-1.53	1.36	0.04	12	0.14	218.5	0.4
47266	201.71099	-47.50966	13.435	11.772	11.160	5198	1.91	-1.41	1.30	0.04	11	0.12	235.4	0.5
47267	201.71148	-47.50817	13.415	11.558	10.914	4927	1.78	-1.82	1.48	0.05	11	0.14	218.8	0.5
47311	201.73819	-47.51253	13.687	11.807	11.136	4872	1.86	-1.78	1.51	0.03	12	0.14	258.1	0.3
47316	201.74130	-47.51007	13.821	99.999	99.999	4920	1.94	-2.08	1.48	0.06	12	0.15	207.5	0.3
47393	201.81548	-47.51007	14.157	12.611	12.090	5470	2.31	-1.72	1.13	0.06	10	0.14	240.4	0.4
47448	201.94348	-47.50712	14.305	12.462	11.839	4967	2.15	-1.69	1.45	0.03	10	0.14	245.3	0.3
48029	201.47784	-47.51702	13.550	11.590	10.962	4831	1.79	-1.70	1.54	0.04	12	0.14	230.2	0.3
48062	201.57397	-47.51703	14.050	12.229	11.634	5024	2.08	-1.73	1.41	0.04	12	0.14	255.2	0.4
48142	201.65953	-47.51643	13.968	12.353	11.814	...	...	...	...	...	...	...	222.1	1.6
48184	201.68407	-47.51507	12.949	11.093	10.534	5025	1.64	-1.79	1.41	0.02	11	0.13	226.1	0.3
48190	201.68754	-47.51754	14.437	13.019	12.467	...	...	...	...	...	...	...	220.3	0.4
48204	201.69542	-47.51590	13.579	11.788	11.151	5011	1.88	-1.72	1.42	0.05	11	0.14	240.5	0.4
48412	201.93998	-47.51807	14.217	12.347	11.733	4946	2.11	-1.63	1.47	0.04	12	0.14	252.1	0.3
49021	201.39712	-47.52855	13.758	11.991	11.396	5089	1.99	-1.87	1.37	0.03	13	0.14	243.4	1.8
49040	201.49012	-47.52444	14.254	12.350	11.763	4937	2.12	-1.55	1.47	0.03	11	0.14	228.5	0.3
49051	201.53067	-47.52571	14.314	12.509	11.966	5107	2.22	-1.66	1.36	0.03	11	0.14	238.8	0.3
49096	201.62228	-47.52650	12.813	10.808	10.095	4698	1.42	-1.96	1.63	0.03	11	0.14	225.3	0.3
49112	201.63467	-47.52379	14.386	12.932	12.465	...	...	...	...	...	...	...	216.2	2.4
49227	201.73050	-47.52874	14.222	12.698	11.847	5078	2.17	-2.37	1.38	0.03	8	0.14	216.2	0.5
50014	201.39736	-47.53208	13.783	11.838	11.162	4797	1.86	-1.78	1.56	0.03	13	0.14	225.8	0.4
50032	201.48996	-47.53682	14.278	12.442	11.826	4983	2.15	-1.76	1.44	0.05	9	0.14	234.3	0.6
50059	201.57049	-47.53784	14.428	12.610	12.012	5024	2.23	-1.71	1.41	0.05	10	0.14	229.9	0.3
50229	201.75250	-47.53363	14.298	99.999	99.999	...	...	...	...	...	...	...	241.3	0.1
50282	201.81909	-47.53666	14.473	12.818	12.340	5379	2.40	-1.22	1.19	0.04	12	0.12	246.4	0.1
50313	201.95036	-47.53040	14.256	12.397	11.746	4917	2.11	-1.63	1.48	0.05	12	0.14	246.4	0.3
50322	202.01013	-47.53630	14.197	12.333	11.668	4896	2.08	-1.79	1.50	0.04	11	0.14	250.9	0.4
51010	201.28295	-47.54029	13.538	11.613	10.922	4802	1.77	-1.84	1.56	0.03	12	0.13	243.1	0.3
51028	201.49361	-47.53882	14.335	12.886	12.165	5335	2.32	-2.39	1.21	0.03	7	0.13	223.3	0.3
51031	201.50104	-47.53942	13.442	11.452	10.794	4768	1.71	-1.85	1.58	0.03	12	0.14	239.4	1.6
51032	201.51265	-47.53860	14.114	12.290	11.691	5016	2.10	-1.72	1.42	0.03	9	0.14	223.7	0.3
51040	201.54198	-47.54162	14.162	12.335	11.699	4970	2.10	-1.71	1.45	0.05	13	0.14	221.8	0.3
51046	201.55975	-47.53970	14.394	12.504	11.861	4891	2.15	-1.44	1.50	0.02	10	0.12	225.5	0.7
51085	201.64340	-47.53882	13.796	12.163	11.641	5351	2.12	-1.88	1.20	0.05	10	0.14	213.3	0.3
51108	201.67527	-47.53969	14.027	12.044	11.406	...	...	...	...	...	...	...	217.2	0.7
51177	201.74708	-47.54476	14.150	12.489	11.988	...	...	...	...	...	...	...	260.8	0.5
51239	201.87329	-47.53890	14.307	12.437	11.835	4959	2.15	-1.90	1.46	0.03	11	0.14	233.9	0.4
51267	201.98687	-47.54246	14.327	12.449	11.831	4932	2.15	-1.78	1.47	0.04	11	0.14	244.3	0.8
52019	201.40733	-47.54643	14.265	12.353	11.737	4896	2.11	-1.61	1.50	0.04	11	0.14	242.0	0.5

**Table 1** *continued*

**Table 1** (*continued*)

LEID	RA	DEC	V	J	K <sub>S</sub>	T <sub>eff</sub>	log(g)	[Fe/H]	$\xi_{\text{mic.}}$	$\sigma/\sqrt{N}$	N	$\Delta[\text{Fe}/\text{H}]$	RV <sub>Helio.</sub>	Error
	(degrees)	(degrees)	(mag.)	(mag.)	(mag.)	(K)	(cgs)	(dex)	(km s <sup>-1</sup> )	(dex)	(dex)	(km s <sup>-1</sup> )	(km s <sup>-1</sup> )	
52025	201.47100	-47.54838	14.489	12.582	11.982	4920	2.21	-1.67	1.48	0.04	11	0.14	236.0	0.8
52037	201.53966	-47.54875	14.424	12.981	12.526	...	...	...	...	...	...	...	237.3	1.1
52041	201.55465	-47.54696	13.798	12.035	11.458	5117	2.02	-1.64	1.35	0.03	11	0.14	218.8	0.5
52043	201.56430	-47.55214	14.444	12.644	12.093	5103	2.27	-1.59	1.36	0.03	10	0.14	223.7	1.2
52045	201.56806	-47.55065	14.118	12.319	11.687	5007	2.10	-1.74	1.43	0.03	13	0.14	216.2	0.4
52082	201.62810	-47.55199	13.765	12.065	11.519	5233	2.06	-1.77	1.28	0.03	11	0.14	226.2	0.4
52118	201.68085	-47.54927	14.093	12.324	11.742	5104	2.13	-1.42	1.36	0.04	10	0.12	242.1	0.3
53025	201.45390	-47.55708	14.388	12.426	11.779	4809	2.11	-1.66	1.55	0.03	11	0.14	234.1	1.3
53032	201.48967	-47.55965	14.390	12.637	11.995	5050	2.23	-1.91	1.40	0.04	10	0.14	235.3	1.8
53050	201.56889	-47.55654	14.328	12.555	11.990	5119	2.23	-1.39	1.35	0.04	10	0.12	249.5	0.4
53082	201.64826	-47.55623	13.836	12.219	11.697	5372	2.14	-1.45	1.19	0.03	13	0.12	231.1	0.3
53180	201.83751	-47.55401	14.038	12.597	12.116	...	...	...	...	...	...	...	241.4	0.4
53200	201.95580	-47.55700	13.405	11.568	10.946	4975	1.80	-1.79	1.45	0.03	10	0.14	242.4	0.3
54037	201.53744	-47.56313	14.001	12.358	11.924	...	...	...	...	...	...	...	225.1	1.7
54041	201.54282	-47.56370	14.280	12.459	11.874	5036	2.18	-1.77	1.41	0.04	13	0.14	238.8	0.4
54044	201.55257	-47.56216	14.488	12.712	12.080	5035	2.26	-1.70	1.41	0.03	9	0.13	231.2	1.0
54050	201.57163	-47.56129	13.413	11.642	11.054	5093	1.85	-1.76	1.37	0.04	12	0.14	231.0	0.3
54125	201.74154	-47.56530	14.486	12.746	12.130	5097	2.29	-1.74	1.37	0.03	9	0.14	253.9	0.3
54146	201.76961	-47.56391	13.520	11.756	11.178	5115	1.91	-1.90	1.36	0.03	10	0.14	219.2	0.5
54181	201.88319	-47.56176	14.168	12.356	11.718	4985	2.11	-1.65	1.44	0.03	10	0.14	251.8	0.4
55012	201.30233	-47.57475	14.472	12.573	11.954	4908	2.19	-1.65	1.49	0.03	10	0.14	246.2	0.3
55042	201.55485	-47.56928	14.075	12.203	11.582	4936	2.05	-1.84	1.47	0.04	10	0.14	231.4	0.8
55049	201.58400	-47.57140	14.130	12.340	11.726	5039	2.12	-1.74	1.40	0.03	10	0.14	235.2	0.4
55077	201.66220	-47.57002	14.389	12.630	12.016	5076	2.24	-1.67	1.38	0.04	12	0.14	254.8	0.9
55158	201.90458	-47.56882	14.182	12.388	11.773	5033	2.14	-1.88	1.41	0.04	11	0.14	215.4	0.9
55164	201.92870	-47.57214	14.240	12.400	11.777	4970	2.13	-1.91	1.45	0.05	9	0.14	241.9	0.6
56037	201.54433	-47.58036	14.024	12.231	11.573	4984	2.05	-1.65	1.44	0.03	10	0.14	228.2	0.6
56042	201.56000	-47.58253	13.284	11.443	10.835	4986	1.76	-1.75	1.44	0.05	11	0.14	218.2	0.3
56098	201.74012	-47.57588	13.583	11.719	11.064	4907	1.84	-1.66	1.49	0.04	11	0.14	257.3	0.4
56132	201.83768	-47.58037	13.296	11.366	10.673	4795	1.67	-1.73	1.56	0.04	10	0.14	238.3	0.3
57015	201.33044	-47.58518	13.749	11.798	11.141	4810	1.86	-1.89	1.55	0.02	12	0.13	237.4	0.3
57022	201.45888	-47.58740	14.291	12.383	11.794	4931	2.13	-1.80	1.47	0.06	10	0.14	226.8	0.4
57024	201.47709	-47.58522	14.497	12.665	12.082	5025	2.26	-1.79	1.41	0.03	11	0.14	236.9	0.8
57033	201.56192	-47.58920	12.646	10.703	10.036	...	...	...	...	...	...	...	235.5	1.4
57036	201.58403	-47.58583	13.878	12.342	11.843	...	...	...	...	...	...	...	235.0	0.3
57046	201.62135	-47.58582	13.609	11.909	11.322	5183	1.97	-1.79	1.31	0.03	9	0.14	243.9	0.3
57102	201.80102	-47.58615	13.762	12.138	11.559	...	...	...	...	...	...	...	244.1	0.5
58052	201.67242	-47.59132	14.241	12.411	11.781	4974	2.13	-1.80	1.45	0.04	11	0.14	225.9	0.6
58063	201.70190	-47.59772	13.680	11.969	11.404	5196	2.01	-1.71	1.30	0.01	8	0.13	226.3	1.3

**Table 1** *continued*

**Table 1** (*continued*)

LEID	RA	DEC	V	J	K <sub>S</sub>	T <sub>eff</sub>	log(g)	[Fe/H]	ξ <sub>mic.</sub>	σ/√N	N	Δ[Fe/H]	RV <sub>Helio.</sub>	Error
	(degrees)	(degrees)	(mag.)	(mag.)	(mag.)	(K)	(cgs)	(dex)	(km s <sup>-1</sup> )	(dex)	(dex)	(dex)	(km s <sup>-1</sup> )	(km s <sup>-1</sup> )
58110	201.97838	-47.59468	14.407	12.516	11.894	4913	2.17	-1.58	1.49	0.03	13	0.14	245.5	0.3
59051	201.69281	-47.60028	14.451	12.715	12.110	5117	2.28	-1.71	1.35	0.04	9	0.14	234.5	0.3
60042	201.59675	-47.60921	14.351	12.562	11.951	5044	2.21	-1.69	1.40	0.03	11	0.14	237.7	0.3
60046	201.61021	-47.61211	14.041	11.913	11.510	4890	2.01	-1.67	1.50	0.04	10	0.14	240.8	2.1
60049	201.61766	-47.60890	13.364	11.566	10.976	5058	1.82	-1.83	1.39	0.03	10	0.14	239.6	0.5
60083	201.78864	-47.60989	13.592	12.122	11.638	...	...	...	...	...	...	...	238.0	0.4
60090	201.82755	-47.60608	14.141	12.246	11.652	4940	2.08	-1.84	1.47	0.05	11	0.14	225.3	1.5
60102	202.00752	-47.60517	13.849	11.914	11.238	4807	1.89	-1.57	1.55	0.04	12	0.14	241.9	0.3
61009	201.16032	-47.61620	13.496	11.533	10.890	4812	1.76	-1.79	1.55	0.05	10	0.14	239.0	0.3
61033	201.50668	-47.61997	14.157	12.256	11.603	4868	2.05	-1.55	1.52	0.03	13	0.14	233.4	0.3
61060	201.68778	-47.61749	14.034	12.206	11.611	5016	2.07	-1.74	1.42	0.04	11	0.14	245.6	0.7
61066	201.70629	-47.61632	14.071	12.620	12.149	...	...	...	...	...	...	...	223.7	0.5
61097	201.90081	-47.61942	14.378	12.493	11.869	4918	2.16	-1.82	1.48	0.04	10	0.14	251.3	0.5
61108	202.01601	-47.61328	14.387	12.529	11.928	4974	2.19	-1.45	1.45	0.04	13	0.12	238.2	0.4
62017	201.42814	-47.62581	14.319	12.478	11.886	5004	2.18	-1.68	1.43	0.05	10	0.14	237.1	0.5
62020	201.47093	-47.62440	14.224	12.524	11.946	5194	2.22	-1.23	1.30	0.05	10	0.12	245.5	0.3
62032	201.58416	-47.62839	13.819	12.134	11.595	5261	2.09	-1.96	1.26	0.07	9	0.15	233.0	0.9
62037	201.65559	-47.62419	13.720	12.020	11.417	5163	2.01	-1.77	1.32	0.04	10	0.14	227.3	1.4
62040	201.67039	-47.62541	14.315	12.942	12.494	...	...	...	...	...	...	...	219.3	0.5
62057	201.77140	-47.62317	13.803	12.134	11.555	5231	2.07	-1.75	1.28	0.03	11	0.14	232.1	0.2
63016	201.41210	-47.63108	14.415	12.548	11.914	4927	2.18	-1.67	1.48	0.03	10	0.14	228.3	0.7
63023	201.45965	-47.63408	14.409	12.598	12.014	5049	2.23	-1.21	1.40	0.04	13	0.12	229.8	0.8
63033	201.63483	-47.62931	14.249	12.491	11.858	5055	2.17	-1.68	1.39	0.05	12	0.14	239.2	0.1
63066	201.90607	-47.63452	14.195	12.560	12.027	...	...	...	...	...	...	...	239.7	0.5
64015	201.42154	-47.63920	13.776	11.859	11.199	4843	1.88	-1.88	1.53	0.03	9	0.14	230.8	0.3
65043	201.73680	-47.64760	13.592	11.894	11.306	5184	1.97	-1.74	1.31	0.04	9	0.14	234.0	1.1
65050	201.82334	-47.64782	14.498	12.690	12.125	5075	2.28	-1.69	1.38	0.04	11	0.14	227.9	1.3
65064	201.98375	-47.64622	13.623	11.750	11.124	4929	1.86	-1.86	1.48	0.03	10	0.14	244.9	0.4
66036	201.66758	-47.65382	13.545	11.740	11.160	5061	1.89	-1.79	1.39	0.04	10	0.14	227.7	0.8
67024	201.48737	-47.66483	14.097	12.514	12.016	5450	2.27	-1.83	1.14	0.04	11	0.14	240.5	0.4
67061	201.92552	-47.65901	14.044	12.399	11.872	5328	2.21	-1.75	1.22	0.03	10	0.14	231.1	0.4
68012	201.45530	-47.67380	13.819	11.929	11.252	4855	1.91	-1.84	1.52	0.04	11	0.14	232.6	0.3
68042	201.69650	-47.66772	13.878	12.278	11.771	5415	2.17	-1.32	1.16	0.06	11	0.13	246.4	0.3
68058	201.95519	-47.67270	14.284	12.654	12.091	...	...	...	...	...	...	...	229.6	0.7
69022	201.59596	-47.67690	13.606	11.903	11.314	5176	1.97	-1.78	1.32	0.05	10	0.14	233.1	1.3
69029	201.67483	-47.67970	13.966	12.109	11.514	4982	2.03	-1.46	1.44	0.03	12	0.12	231.3	0.4
70018	201.46893	-47.68703	14.348	12.500	11.899	4986	2.18	-1.65	1.44	0.03	11	0.14	233.3	0.3
70021	201.50974	-47.68662	14.229	12.390	11.749	4951	2.12	-1.74	1.46	0.03	10	0.14	237.0	0.3
70034	201.64550	-47.68823	14.696	12.910	12.339	5095	2.37	-1.72	1.37	0.04	10	0.14	230.9	0.5

**Table 1** *continued*

**Table 1** (*continued*)

LEID	RA	DEC	V	J	K <sub>S</sub>	T <sub>eff</sub>	log(g)	[Fe/H]	$\xi_{\text{mic.}}$	$\sigma/\sqrt{N}$	N	$\Delta[\text{Fe}/\text{H}]$	RV <sub>Helio.</sub>	Error
	(degrees)	(degrees)	(mag.)	(mag.)	(mag.)	(K)	(cgs)	(dex)	(km s <sup>-1</sup> )	(dex)	(dex)	(km s <sup>-1</sup> )	(km s <sup>-1</sup> )	
71007	201.16956	-47.69628	14.175	12.902	12.481	...	...	...	...	...	...	...	245.4	0.4
72030	201.78780	-47.70323	14.204	12.379	11.737	4966	2.11	-1.77	1.45	0.04	11	0.14	224.9	0.9
72036	201.88234	-47.70068	14.524	12.697	12.096	5010	2.26	-1.61	1.42	0.04	11	0.14	244.1	0.4
72038	201.88711	-47.69996	14.342	12.459	11.807	4889	2.13	-1.71	1.50	0.03	11	0.14	234.8	0.5
73023	201.55469	-47.70494	13.879	12.002	11.316	4859	1.93	-1.69	1.52	0.03	12	0.14	235.3	0.3
74022	201.50340	-47.71515	14.383	12.504	11.891	4937	2.17	-1.75	1.47	0.05	11	0.14	234.8	0.3
75016	201.49426	-47.72636	13.599	11.609	10.925	4742	1.76	-1.90	1.60	0.02	11	0.13	243.7	0.6
76040	201.86016	-47.73142	14.474	12.643	12.021	4981	2.23	-1.69	1.44	0.04	13	0.14	243.8	0.4
77013	201.39428	-47.74240	14.377	12.595	12.011	...	...	...	...	...	...	...	241.3	3.8
78019	201.60662	-47.74807	14.385	12.586	11.940	4991	2.20	-1.65	1.44	0.03	11	0.14	241.2	0.6
79014	201.51713	-47.75403	14.302	12.443	11.762	4884	2.11	-1.59	1.50	0.03	13	0.14	232.1	0.4
79026	201.68852	-47.74982	14.046	12.139	11.505	4882	2.01	-1.69	1.51	0.03	10	0.14	212.0	0.5
80031	201.73648	-47.76091	14.071	12.187	11.547	4901	2.03	-1.43	1.49	0.02	13	0.12	227.0	0.4
80036	201.89616	-47.76113	13.819	11.850	11.187	4785	1.87	-1.82	1.57	0.03	12	0.14	229.3	0.7
82026	201.76406	-47.77511	14.217	12.290	11.632	4835	2.06	-1.65	1.54	0.03	11	0.14	246.6	1.1
82028	201.77773	-47.77823	14.335	12.458	11.809	4899	2.13	-1.84	1.50	0.05	9	0.14	236.9	1.2
82031	201.83208	-47.77207	14.319	12.684	12.130	...	...	...	...	...	...	...	227.5	0.5
83020	201.54861	-47.78255	14.300	12.449	11.835	4968	2.15	-1.68	1.45	0.05	10	0.14	237.9	0.6
84013	201.68779	-47.79316	13.658	11.697	11.030	4789	1.81	-1.68	1.57	0.03	12	0.14	247.3	0.4
89014	201.66544	-47.83110	13.607	11.639	10.967	4777	1.78	-1.53	1.57	0.04	13	0.14	231.3	0.4
90019	201.62529	-47.83825	13.509	11.537	10.911	4820	1.77	-1.76	1.55	0.04	13	0.14	231.2	0.6
90026	201.88385	-47.83773	13.958	12.049	11.392	4855	1.96	-1.56	1.52	0.04	13	0.14	224.5	1.2
92026	201.83944	-47.84879	13.600	11.778	11.184	5024	1.90	-1.84	1.41	0.05	11	0.14	232.3	0.3
93016	201.65058	-47.86211	14.479	12.620	12.031	4987	2.23	-1.54	1.44	0.04	13	0.14	231.5	0.3
96011	201.52316	-47.88203	12.975	11.027	10.416	4862	1.57	-1.79	1.52	0.03	10	0.14	228.7	0.4
98012	201.35549	-47.89600	13.623	12.034	11.471	5355	2.05	-1.67	1.20	0.04	11	0.14	228.6	0.9



**Table 2.** Fe I Line List

Wavelength (Å)	E.P. (eV)	$\log g f$
5141.739	2.422	-2.00
5145.094	2.196	-3.06
5150.839	0.989	-3.07
5159.058	4.280	-0.65
5198.711	2.221	-1.97
5213.344	4.383	-2.18
5216.274	1.607	-2.15
5242.491	3.632	-0.84
5243.776	4.253	-0.90
5247.050	0.087	-4.65
5288.527	3.692	-1.54
5321.108	4.431	-1.24
5322.041	2.277	-2.85
5379.574	3.692	-1.42